



Steady MHD Casson Ohmic heating and viscous dissipative fluid flow past an infinite vertical porous plate in the presence of Soret, Hall, and ion-slip current

K. V. B. Rajakumar¹  | M. Umasankara Reddy¹  |
K. S. Balamurugan² | K. V. B. S. Raja Ram³

¹Department of Mathematics, Kallam Haranadhareddy Institute of Technology, Guntur, India

²Department of Mathematics, R. V. R. & J. C. College of Engineering, Guntur, India

³Department of Mathematics, P. R. S. M. National College, Gudivada, India

Correspondence

K. V. B. Rajakumar, Department of Mathematics, Kallam Haranadhareddy Institute of Technology, Guntur, Andhra Pradesh 522109, India.

Email: kvbrajakumar@gmail.com

Abstract

In the present study, the influence of Hall and ion-slip current on steady magnetohydrodynamics mixed convective, Ohmic heating, and viscous dissipative Casson fluid flow over an infinite vertical porous plate in the presence of Soret effect and chemical reaction are investigated. The modeling equations are transformed into dimensionless equations and then solved analytically through the multiple regular perturbation law. Computations are performed graphically to analyze the behavior of fluid velocity, temperature, concentration, skin friction, Nusselt number, and Sherwood number on the vertical plate with the difference of emerging physical parameters. This study reflects that the incremental values of Casson fluid parameter and Schmidt number lead to reduction in velocity. However, fluid velocity rises due to enhancement of ion-slip parameter but an opposite effect is observed in case of Hall parameter. In addition, the Sherwood number declines with enhancing dissimilar estimators of the chemical reaction, Schmidt number, as well as Soret number.

KEYWORDS

Casson fluid, Hall and ion-slip current, MHD, multiple regular perturbation law, Ohmic heating

1 | INTRODUCTION

Due to versatile technological as well as engineering applications, it is important to study the magnetohydrodynamics (MHD) flow. The foremost objective of the principles of MHD is to interrupt the flow field in a required direction by fluctuating the formation of the boundary layer. Thus, to modify the flow kinematics, executing MHD seems to be more flexible and reliable. In pharmaceutical as well as environmental sciences, MHD plays a vital role in the application of fluid dynamics and medical sciences, due to its implications in chemical and metallurgical fields. The collective influence of fluid dynamics and thermodynamics along with electrodynamics empowers going up to the topic of magnetic field dependent (MFD). It is divided into two types: MHD and magneto gas dynamic (MGD). MHD addresses electrically conducting fluids while MGD deals with ionized compressible gases. There are several beneficial applications of MHD free convection flows in fiber as well as granular insulation, geothermal systems, fusion research, MHD accelerators, power generators, and so on. MHD fluid flow in fluid mechanics has been studied by a significant number of mathematicians, engineers, scientists, as well as researchers under various conditions, such as Biswas et al^{1,2} and Ahmmed et al³.

Non-Newtonian fluid flow has found applications in several fields of modern technological and engineering chemical material production processes. There are various kinds of non-Newtonian fluids, such as couple stress fluid, power-law fluid, viscoelastic fluid, microplar fluid, Maxwell fluid, and so on. Besides these, there is one more well-known non-Newtonian fluid model called the Casson fluid model. It is a major component of pseudoplastic fluids that was propounded by Casson in 1995. On the other hand, several industrial fluids like paints, granular suspension, polymer solutions shampoos, slurries, paper pulp, drilling muds, as well as certain oils are of non-Newtonian nature. The effect of non-Newtonian boundary layer flow in the case of vertical porous plates has remarkable applications in several industrial as well as manufacturing processes. Several researchers have focused on the investigation of distinct non-Newtonian fluid models in reference to various physical conditions. Compared to all the above-stated non-Newtonian fluid models, the Casson fluid model has two advantages. First, it is derived from the kinetic theory of liquid rather than the experimental relation as in the case of Casson fluid model. Second, it diminishes to Newtonian nature at bound shear rates. The investigation of Casson fluid flow predominantly in the MHD effect with free convection flow has received substantial attention by several research scholars of the modern era. In the recent times, immense research work has been carried out on the MHD effects of Casson fluid flow, Hall and ion current, Dufour, radiation absorption, viscous dissipation, and chemical reaction through porous plates. John Etwire et al⁴ investigated, numerically, the MHD flow of Casson fluid over a nonparallel plate immersed in porous media by means of Joule heating as well as convective boundary condition. Mittal et al⁵ have addressed a two-dimensional Casson fluid model on mixed convective MHD stagnation point flow past an infinite plate in the presence of a porous medium. They observed that the governing partial differential equations (PDEs) are modulated utilizing similarity transformation and the system of ODE is solved utilizing HAM. Harshad et al⁶ have examined the characteristics of heat and mass transfer on 2-D mixed convection Casson fluid flow past an infinite plate in a porous medium under the influence of a uniform magnetic field and cross-diffusion in the presence of heat generation as well as heat absorption by means of chemical reactions. Kataria et al⁷ analyzed heat and mass transfer in MHD Casson fluid flow past an oscillating vertical plate embedded in porous medium with ramped wall temperature. Vinod Kumar et al⁸ studied steady MHD stagnation Casson fluid flow over a stretching sheet under slip boundary conditions in the presence of a chemical reaction

and Joule heating and analyzed viscous dissipation. Prasad et al⁹ have examined MHD Casson fluid flow over a permeable nonparallel impassioned stretching surface by means of transpiration considering variable fluid properties. Ullah et al¹⁰ studied MHD mixed convection flow of Casson fluid in the presence of a chemical reaction as well as investigated viscous dissipation. In this investigation, Joule heating due to a magnetic field as well as porous medium heating were considered. In this paper, it was observed that velocity reduced due to rising values of Casson parameter and magnetic field parameter. El-Aziz et al¹¹ analyzed the influence of free convection flow on an unsteady Casson fluid over a nonparallel channel. In this paper, the governing equations are solved by using the Laplace transform method. From these results, it was observed that the velocity reduced due to the incremental values of Casson fluid parameter as well as Prandtl number. From this paper, increase in viscous force as well as retardation in the movement of the velocity were observed. Biswas et al¹² investigated a Casson fluid model on an unsteady free convective flow past a nonparallel porous plate in the presence of doubled diffusion, radiation, as well as chemical reaction. In this paper, nondimensional PDEs were solved by utilizing the finite difference technique. Biswas et al¹³ introduced superintendence by means of stability exploration of Casson nanofluid flow in the influence of variable thermal conductivity as well as radiation.

Thermal radiation is important for several applications because of the way in which radiant emission depends on temperature. Subsequently, radiation contributes significantly to energy transfer in furnaces, combustion chambers, fires and to energy emission, such as that of a nuclear explosion. Radiative behavior governs the temperature distribution within the sun and the solar emission. Devices are designed to operate at high temperature levels to achieve good thermal efficiency. Hence radiation must be considered in calculating thermal effects in rocket nozzles, power plants, engines and high-temperature heat exchangers, geophysics, various propulsion devices for missiles, photoionization, gas turbines, combustion of fossil fuels, nuclear power plants, liquid metal fluids, plasma wind tunnels, aircrafts, space vehicles, and satellites. The effects of thermal radiation on MHD free convective fluid over a semi-infinite nonparallel permeable plate under dissimilar flow conditions have been investigated by various researchers. The influence of radiation as well as explicit finite difference on an unsteady MHD double-diffusion transfer micropolar fluid flow with chemical reaction through a normal porous plate has been studied by Biswas et al.¹⁴ Srinivas et al¹⁵ analyzed the effects of thermal radiation, chemical reaction, as well as thermal diffusion on MHD Casson fluid pulsating flow of a porous channel. In this examination, it was found that the fluid was vaccinated from the bottom of the wall as well as sucked out from the overlying wall with identical velocities. In this examination, the fluid concentration was diminished with increase in chemical reaction and Soret number. From this investigation, the results revealed that, for both the Newtonian as well as non-Newtonian cases, the Nusselt number reduced at the overlying wall with incremental values of Hartmann number as well as radiation parameter. Sobamowo et al¹⁶ considered the influence of thermal radiation as well as nanoparticles on free convection flow and investigated heat transfer of Casson nanofluids over a nonparallel plate. In this analysis, it was observed that the velocity as well as temperature rises with increasing values of the thermal radiation parameter. In addition, although the incremental values of Prandtl number and volume fraction led to enhancement in velocity, an inverse effect was observed in case of temperature. Kataria et al¹⁷ reported the influence of heat generation as well as heat absorption on unsteady MHD Casson fluid flow past beyond an exponentially accelerated normal plate inherent in porous medium in the presence of a chemical reaction. In this examination, it was considered that the bounding plate possesses ramped temperature with ramped surface concentration and

isothermal temperature with ramped surface concentration. Radiation along with thermal conductivity on unsteady MHD free convection flow of viscous nanofluid over an exponentially accelerated inclined porous plate by means of variable viscosity has been reported by Ahmmed et al.¹⁸

The problems of steady as well as unsteady double diffusion by free convection along infinite and semi-infinite perpendicular plates with and without chemical reaction have been studied widely by numerous scholars. Chemical reactions can be bifurcated into bi-homogeneous and heterogeneous reactions. A homogeneous reaction acts uniformly through a specified stage. The diversity in heterogeneous reaction acts in a confined area or inside the boundary of a phase. The rate of reaction is proportional to the concentration; this phenomenon reaction is known as first order. A significant chemical reaction between a foreign mass and the fluid is found in many chemical industrial processes. The conglomeration of heat and mass transfer problems with chemical reactions are widely found in the fields of manufacturing of ceramics, polymer production, synthetics fibers, and application of isothiocyanate components in preparing products such as food or drink products, pharmaceutical compositions, agricultural products, skin or hair products, and so on. Vijaya et al¹⁹ analyzed chemical reaction as well as thermophysical properties of MHD Casson fluid through an oscillating nonparallel wall enclosed in a permeable channel and effect of transverse magnetic field and radiation in the presence of a constant heat source. In this paper, the governing equations were solved by using the R-K Fehlberg method by means of a shooting technique. Biswas et al²⁰ focused on impact of hall current along with Casson nanofluid model on unsteady MHD heat and mass transfer flow by way of a vertical plate in the aspect of radiation as well as chemical reaction. Mondal et al²¹ conducted numerical studies by means of stability convergence scrutiny of chemically hydro-mantic Casson nanofluid flow under the influence of thermophoresis and Brownian motion.

In many fluid mechanics problems, destruction of fluctuating velocity gradients due to viscous stresses is called viscous dissipation. In other words, the irreversible process with which the work done by a fluid on contiguous layers owing to the influence of shear forces is changed into heat is called viscous dissipation. This partially irreversible process is frequently mentioned as the metamorphosis of kinetic energy into internal energy of the fluid. The influence of viscous dissipation is very important in geophysical flows, instrumentation, tribology, lubrications, polymer manufacturing as well as in certain engineering operations and it is generally distinguished by Eckert number (Ec). Reddy et al²² investigated unsteady MHD natural convective Casson fluid over an oscillating nonparallel porous plate with double diffusion, by the means of viscous dissipation. From this investigation, it was concluded that the incremental values of porous medium, Grashof number as well as Eckert number lead to enhancement in velocity, but reverse effect was occurred in case of Casson fluid parameter, magnetic field parameter as well as phase angle. Meanwhile, the enhancement of different values of Eckert number lead to reduction in local skin friction. Attia et al²³ reported the implication of viscous dissipation as well as Hall current on unsteady MHD free convective Casson fluid model flow over a double diffusion bounded by bi-analogue nonconducting porous plate. In this analysis, it was established that an external uniform magnetic field was utilized which is perpendicular to the plates as well as the fluid motion, which was subjected to a uniform suction with injection. Srinivasa Raju et al²⁴ reported that the effects of magnetic field as well as viscous dissipative on unsteady MHD free convective Casson fluid flow over a nonparallel inclined plate in presence of double diffusion. In this study, ion-slip and Hall current were inconsequential. Saidulu et al²⁵ investigated the significance of exponentially stretching sheet and Casson fluid model on MHD flow conducted by heat transfer by means of

velocity slip as well as thermal slip conditions in the influence of thermal radiation, viscous dissipation as well as heat source. In this examination, ion-slip current and Hall was insignificant. Recently, an excellent research was explained by Srinivasa Raju et al,²⁶ in which, an investigation was carried out on Casson fluid model by means of viscous dissipative effect on unsteady MHD natural convective double diffusion, electrically conducting flow over a non-parallel surface in presence of angle of inclination with chemical reaction as well as heat flux which is constant. In this paper, it was examined that the results indicates that the incremental values of Eckert number leads to rise in temperature other than inverse effect was occurred in case of Prandtl number. In addition, concentration rises due to enhancement of Soret as well as Schmidt number. In this examination, it was found that finite element method was utilized for solving governing equations. Influence of viscous dissipation on steady MHD Casson fluid flow close to the stationary point over a stretching surface in the existence of the induced magnetic field and magnetic dissipation as well as radiation absorption has been investigated numerically by El-Aziz et al.²⁷

Joule heating, also known as Ohmic heating and resistive heating, is the process by which the channel of an electric current during a conductor generated heat, that is, the power of heating produces by an electrical conductor is relative to the product of its resistance as well as the square of the current. Recently, Abo-Eldahab et al,²⁸ Barletta et al,²⁹ Babu et al,³⁰ and Chien Hsin et al³¹ analyzed Joule as well viscous dissipation as at the same time heat generation has been taken into consideration in the equation of energy. In this study, Casson fluid model as well as Hall and ion slip effects were not considered. Ibrahim et al³² examined steady MHD mixed convective viscous dissipation as well as Joule heating fluid flow past an infinite nonparallel permeable plate by means of chemical reaction and Soret in the presence of heat source. Harshad et al³³ have addressed viscous dissipation as well as Joule heating on mixed convection micropolar fluid flow in porous medium with uniform magnetic field toward nonlinear stretched surface. This examination was carried out in the presence of convective boundary condition, thermophoresis, Brownian motion, chemical reaction, and nonlinear thermal radiation. Akhil et al³⁴ have investigated viscous dissipation and Joule heating on mixed convection micropolar ferrofluid flow in the presence of nonlinear stretched sheet. Analysis of hydromagnetic stability convenience on unsteady double diffusion fluid flow over a vertical porous plate has been examined by Biswas et al.³⁵ In this investigation, Joule and viscous dissipation effects were not considered.

Mass transformation through temperature gradient is known as Soret effect (thermal diffusion). This effect has been widely examined both theoretically as well as experimentally in fluids. These effects are investigated as second-order phenomena. The practical applications for these effects were studied widely in geothermal energy, nuclear desecrate removal, hydrology, as well as petrology, etc. Soret gives in isotope separation process as well as mixture between gasses (H_2 , H_e) of lesser molecular weight and (N_2 , air) of medium molecular weight. Balamurugan et al³⁶ have analyzed influence of thermodiffusion on MHD free convection flow through porous medium by means of constant suction and in the presence of chemical reaction as well as viscous dissipation. Pannerselvi et al³⁷ contributed analytical solution, and influence of sort as well as oscillatory section velocity on unsteady MHD free convective mass transfer flow along with viscous fluid past an infinite nonparallel permeable plate of time dependent with heat source, Hall and ion slip current. Influence of diffusion thermo and rotating system on MHD fluid flow past an infinite moving nonparallel plate by means of on the surface heating as well as cooling of the plate in presence of isothermal along with ramped wall temperature with hall and thermal diffusion have been examined by Abuga et al.³⁸ Odelu Ojjela et al³⁹ and Shateyi et al⁴⁰ discussed significance of Dufour as well as Soret effects on MHD free convective

flow of double diffusion an electrically conducting couple stretch fluid past porous channels by means of chemical reaction and Hall and ion slip current. In the above examination, Casson fluid models were not taken into consideration.

The production of an extrapropective dissimilarity transverse to the direction of accumulate free charge and applied magnetic field (perpendicular to the flow of charge) among the opposite surfaces induces an electric current vertical to both the fields, magnetic as well as electric. This current is known as Hall current. The phenomenon is denominated as Hall effect. In modern days, there is a wide range of applications—from automobiles to aircrafts, medical equipment, and computers to sewing machines, as well as in the field of energy, for instance, Hall accelerators and MHD generators. Numerous investigators have examined Hall current on MHD free convective flows. Patel et al⁴¹ carried out a research on the impact of Hall current and Casson fluid model on MHD natural convection flow of an oscillating perpendicular plate and ramped wall temperature in a rotating system with thermal radiation as well as heat generation in the presence of chemical reaction. Vijayaragavan et al⁴² have examined the significance of Hall current effect on MHD Casson fluid flow in the presence of Dufour as well as thermal radiation effects by means of chemically reaction. In this investigation, perturbation technique has been utilized for solving nonlinear PDEs. From these results, it was observed that the enhancement of dissimilar values of Schmidt number, magnetic parameter, and chemical reaction parameter as well as Prandtl number leads to reduction in skin friction, nevertheless, reverse effect was shown in case of Nusselt number. Anika et al⁴³ and Srinivasacharya et al⁴⁴ have focused on the significance of double diffusion, Hall and ion slip current effects on MHD free convection flow of an electrically conducting couple stretch fluid through permeable channels by means of chemical reaction and Dufour as well as Soret number. In the above literature survey, effects of viscous dissipation and Joule heating have not been considered. Significance of Hall and ion-slip current on MHD free convective Casson fluid flow through vertical oscillatory permeable plate has been discussed by Rajakumar et al.^{45–47}

The objective of the present examination is to investigate the Hall and ion-slip current on MHD mixed convective, Ohmic heating, and viscous dissipative Casson fluid flow over an infinite vertical porous plate in the presence of Soret and chemical reaction. Such examination has noteworthy applications in real world problems and is expected to have a major impact on imperative national requirements. It also improves scientific knowledge, development of novel technologies, improvements to security, defense, and major contributes toward health. Also, it has more applications in transportation, biomedical, scientific measurement, paper manufacturing industries, polymer processing industries, microelectronics and biomechanics, chemical engineering fields, as well as industrialized processes, for instance, metal spinning, nuclear squander repositories, polymer extrusion, material processing, transpiration cooling, strengthen oil recovery products, microfluidics, crammed bed catalytic reactors, continuous casting of metals, glass as well as fiber manufacture and wire drawing, etc. The modelling equations are revolutionized into dimensionless equations and after that solved analytically by utilizing perturbation law. Computations were performed graphically to explain the behavior of fluid velocity, temperature, Concentration as well as skin friction, Nusselt number, Sherwood number with the dissimilarity of emerging physical parameters.

2 | MATHEMATICAL FORMULATION

Consider the two dimensional MHD mixed convective flow of an incompressible and electrically conducting, viscous Casson fluid over a permeable infinite vertical plate with a saturated

porous medium by means of heat and mass transfer in a uniform of a pressure grading. The following assumptions are made:

The rheological equation of state for the Cauchy stress tensor of Casson fluid can be written as $\tau = \tau_0 + \mu\alpha^*$ (Reddy et al²²).

$$\text{Equivalently } \tau_{ij} = \begin{cases} 2 \left[\mu_B + \frac{p_y}{\sqrt{2\pi}} \right] e_{ij} & \pi > \pi_c \\ 2 \left[\mu_B + \frac{p_y}{\sqrt{2\pi_c}} \right] e_{ij} & \pi < \pi_c \end{cases} \quad \pi = e_{ij}e_{ij}, \quad e_{ij} = \text{the } (i, j)^{th} \text{ component of}$$

deformationrate, τ_0 = Casson yield stress, π = the product based on the non-Newtonian fluid, π_c = a critical value of this product, μ_B = plastic dynamic viscosity of the non-Newtonian fluid, μ = the dynamic velocity, α^* = shear rate. $p_y = \frac{\mu_B \sqrt{2\pi}}{\beta}$ = the yield stress of fluid. Some fluids require a gradually increasing shear stress to maintain a constant strain rate and are called rheopectic, in the case of Casson fluid flow. Where $\tau > \tau_c$, $\mu = \mu_B + \frac{p_y}{\sqrt{2\pi}}$. Finally, $\beta = \frac{\mu_B \sqrt{2\pi_c}}{p_y}$ is the Casson fluid parameter.

In this exploration, an account of that x^* -axis is taken along the plate in upward direction and y^* -axis is in the direction of orthogonal to the flow (see Figure 1). Supposed that transverse magnetic field of the uniform strength B_0 is to be utilized in the direction of y^* -axis. Given that the motion is two-dimensional and moreover, length of the plate is large, therefore all the physical variables are independent of x^* . u^* and v^* are the dimensional velocities components along x^* and y^* directions. Joule, viscous dissipation, and heat generation are considered in the equation of energy; at the same time, kinematic viscosity is considered in the equation of momentum. Since uniform magnetic field B is performed transverse the plate. By means of the relation $\nabla B = 0$ or $B = (B_x, B_y, B_z)$, $B_y = 0$ has been consider everywhere in the fluid, B_0 is constant. If $J = (J_x, J_y, J_z)$ is the current density, from the relation $\nabla J = 0$, $J_y = \text{constant}$ has been obtained. Given that the plate is electrically nonconducting, $J_y = 0$ at the plate, and therefore zero ubiquitously. When the strength of magnetic field is very huge, the generalized Ohm's law for the current in the form current in the form:

$$\bar{J} = \sigma \left(1 + \left(\omega \left(\frac{1}{J_e} \right) \right)^2 \right)^{-1} (\bar{E} + (\bar{V} \times \bar{B}) - \left(\frac{1}{en_e} \right) (\bar{J} \times \bar{B})),$$

Here ω = electron cyclotron. ϑ_e = electron-atom collision frequency. When the ratio $\omega(\vartheta_e)^{-1}$ is very huge, the phenomenon is called “ion-slip”. The homogeneous chemical reaction is of first order with rate constant between the diffusing species and Soret effect is considered.

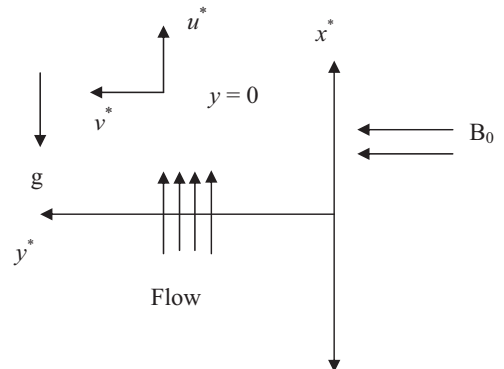


FIGURE 1 Physical model of the problem

From the above assumptions, the unsteady flow is governed by the following partial differential equations.

Equation of continuity:

$$\frac{\partial v^*}{\partial y^*} = 0. \quad (1)$$

That is, $v^* = \text{constant} = -v_0$

Equation of momentum:

$$v^* \left[\frac{\partial u^*}{\partial y^*} \right] = \vartheta \left[1 + \frac{1}{\beta} \right] \left[\frac{\partial^2 u^*}{\partial y^{*2}} \right] + v_r \left[\frac{\partial^2 u^*}{\partial z^{*2}} \right] + g\beta [T^* - T_\infty] + g\beta^* [C^* - C_\infty] - \frac{v_r}{K^*} [u^*] - \frac{\vartheta}{K^*} \left[1 + \frac{1}{\beta} \right] u^* - \frac{B_0^2 \sigma_e [\alpha_e u^* + \beta_e w^*]}{\rho [\alpha_e^2 + \beta_e^2]}, \quad (2)$$

$$v^* \left[\frac{\partial w^*}{\partial y^*} \right] = \vartheta \left[1 + \frac{1}{\beta} \right] \left[\frac{\partial^2 w^*}{\partial y^{*2}} \right] + v_r \left[\frac{\partial^2 w^*}{\partial z^{*2}} \right] - \frac{\vartheta}{k^*} \left[1 + \frac{1}{\beta} \right] [w^*] - \frac{v_r}{K^*} w^* + \frac{B_0^2 \sigma_e [\beta_e u^* - \alpha_e w^*]}{\rho [\alpha_e^2 + \beta_e^2]}. \quad (3)$$

Equation of energy:

$$v^* \left[\frac{\partial T^*}{\partial y^*} \right] = \frac{k}{\rho C_p} \left[\frac{\partial^2 T^*}{\partial y^{*2}} \right] + \frac{Q_0}{\rho C_p} [T^* - T_\infty] + \left[1 + \frac{1}{\beta} \right] \left(\frac{\vartheta}{C_p} \left(\left(\frac{\partial u^*}{\partial y^*} \right)^2 + \left(\frac{\partial w^*}{\partial y^*} \right)^2 \right) + \frac{B_0^2 \sigma_e}{[\alpha_e^2 + \beta_e^2] \rho C_p} (u^{*2} + w^{*2}) \right). \quad (4)$$

Equation of concentration:

$$v^* \left[\frac{\partial C^*}{\partial y^*} \right] = D \left[\frac{\partial^2 C^*}{\partial y^{*2}} \right] + D_1 \left[\frac{\partial^2 T^*}{\partial y^{*2}} \right] - k_1 [C^* - C_\infty]. \quad (5)$$

The corresponding boundary conditions of the problem

$$\left. \begin{aligned} u &= 0, \quad T^* = T_w, \quad C^* = C_w \quad \text{at } y = 0 \\ u &\rightarrow 0, \quad T^* \rightarrow T_\infty, \quad C^* = C_\infty \quad \text{as } y \rightarrow \infty \end{aligned} \right\} \quad (6)$$

Let us introduce the following dimensionless quantities in the Equations (2)–(5). Then, we get:

$$f(\eta) = \frac{u^*}{v_0}, \quad g(\eta) = \frac{w^*}{v_0}, \quad \eta = \frac{v_0 y^*}{\vartheta}, \quad \theta = \frac{(T^* - T_\infty)}{(T_w - T_\infty)}, \quad \phi = \frac{(C^* - C_\infty)}{(C_w - C_\infty)}, \quad (7)$$

$$\left[1 + \frac{1}{\beta} + \gamma\right] f'' + f' - K_0 \left[1 + \frac{1}{\beta} + \gamma\right] [u] - \frac{M[\alpha_e f + \beta_e g]}{[\alpha_e^2 + \beta_e^2]} + Gr\theta + Gm\phi = 0, \quad (8)$$

$$\left[1 + \frac{1}{\beta} + \gamma\right] g'' + g' - K_0 \left[1 + \frac{1}{\beta} + \gamma\right] [g] + \frac{M[\beta_e f - \alpha_e g]}{[\alpha_e^2 + \beta_e^2]} = 0, \quad (9)$$

$$\theta'' + Pr\theta' = -Ec \operatorname{Pr} \left[1 + \frac{1}{\beta}\right] \left[((f')^2 + (g')^2) - \frac{M^2}{[\alpha_e^2 + \beta_e^2]} (f^2 + g^2) \right] - Q \operatorname{Pr} \theta, \quad (10)$$

$$\phi'' + Sc\phi' - Kr Sc\phi = -So Sc\theta, \quad (11)$$

The relevant boundary conditions are:

$$\left. \begin{aligned} \eta = 0: f = 0, \quad g = 0, \quad \theta = 1, \quad \phi = 1 \\ \eta \rightarrow \infty: f \rightarrow 0, \quad g \rightarrow 0, \quad \theta \rightarrow 0, \quad \phi \rightarrow 0 \end{aligned} \right\} \quad (12)$$

$$\left. \begin{aligned} \operatorname{Pr} = \frac{\vartheta \rho C_p}{k}, \quad Sc = \frac{\vartheta}{D}, \quad k_r = \frac{\vartheta k_1}{v_0^2}, \quad \vartheta = \frac{\mu}{\rho}, \quad Gr = \frac{\vartheta g \beta (T_w - T_\infty)}{v_0^3}, \quad k^* = \frac{\vartheta}{v_0^2 K_0} \\ So = \frac{D_1(T_w - T_\infty)}{\vartheta(C_w - C_\infty)}, \quad M^2 = \frac{\sigma B_0^2 \vartheta}{\rho v_0^2}, \quad \gamma = \frac{v_r}{\vartheta}, \quad Gm = \frac{\vartheta g \beta^*(C_w - C_\infty)}{v_0^3} \\ Ec = \frac{v_0^2}{C_p(T_w - T_\infty)}, \quad Q = \frac{Q_0}{C_p \rho v_0^2}, \quad N = \left[\left[1 + \frac{1}{\beta} + \gamma\right] K_0 + \frac{M^2[-\alpha_e + i\beta_e]}{[\alpha_e^2 + \beta_e^2]} \right] \end{aligned} \right\}, \quad (13)$$

Equations (8) and (9) are displayed, in a reduced form, as

$$\left[1 + \frac{1}{\beta} + \gamma\right] F'' + F' - N[F] = -Gr\theta - Gm\phi, \quad (14)$$

$$\theta'' + \operatorname{Pr}\theta' = -Ec \operatorname{Pr} \left[1 + \frac{1}{\beta}\right] \left[\left(\frac{\partial F}{\partial \eta} \frac{\partial \bar{F}}{\partial \eta} \right) - \frac{M^2}{[\alpha_e^2 + \beta_e^2]} (F\bar{F}) \right] - Q \operatorname{Pr} \theta. \quad (15)$$

The relevant boundary conditions are:

$$\left. \begin{aligned} \eta = 0: F = 0, \quad \theta = 1, \quad \phi = 1 \\ \eta \rightarrow 0: F \rightarrow 0, \quad \theta \rightarrow 0, \quad \phi \rightarrow 0 \end{aligned} \right\} \quad (16)$$

$$\text{Where } F = f + ig, \quad i = \sqrt{-1}. \quad (17)$$

3 | METHOD OF SOLUTION

The resulting system of nonlinear ODEs (11), (14), and (15) subjected to the boundary conditions presented in Equation (16) has been explored numerically through the multiple regular perturbation law. The physical variables F , θ , and ϕ are expanded in the power of Eckert number (Ec). This can be achieved physically as Ec for the flow of an incompressible fluid is always less than unity. It can be seen physically as the flow due to the Joule as well as viscous dissipation is super inflicting on the main flow. In this examination, only the real part is discussed. Hence, we can assume:

$$\left. \begin{aligned} F(\eta) &= F_0(\eta) + Ec F_1(\eta) + O(Ec)^2... \\ \theta(\eta) &= \theta_0(\eta) + Ec \theta_1(\eta) + O(Ec)^2... \\ \phi(\eta) &= \phi_0(\eta) + Ec \phi_1(\eta) + O(Ec)^2... \end{aligned} \right\} \quad (18)$$

Using Equation (18) in Equations (11), (14) and (15) and equating the coefficient of similar powers of Ec , we have,

$$\left[1 + \frac{1}{\beta} + \gamma \right] F_0'' + F_0'' - NF_0 = -Gr\theta_0 - Gm\phi_0, \quad (19)$$

$$\left[1 + \frac{1}{\beta} + \gamma \right] F_1'' + F_1' - NF_1 = -Gr\theta_1 - Gm\phi_1, \quad (20)$$

$$\theta_0'' + Pr\theta_0' + QPr\theta_0 = 0, \quad (21)$$

$$\theta_1'' + Pr\theta_1' + QPr\theta_1 = -Pr \left[1 + \frac{1}{\beta} \right] (F_0')^2 - Pr \left[\frac{M^2}{\alpha_e^2 + \beta_e^2} \right] \left[1 + \frac{1}{\beta} \right] F_0^2, \quad (22)$$

$$\phi_0'' + Sc\phi_0' - KrSc\phi_0 = -ScSo\theta_0'', \quad (23)$$

$$\phi_1'' + Sc\phi_1' - KrSc\phi_1 = -ScSo\theta_1''. \quad (24)$$

Subject to the boundary conditions

$$\left. \begin{aligned} \text{at } \eta = 0: & \quad F_0 = 0, \quad F_1 = 0, \quad \theta_0 = 1, \quad \theta_1 = 0, \quad \varphi_0 = 1, \quad \varphi_1 = 0 \\ \text{as } \eta \rightarrow \infty: & \quad F_0 \rightarrow 0, \quad F_1 \rightarrow 0, \quad \theta_0 \rightarrow 0, \quad \theta_1 \rightarrow 0, \quad \varphi_0 \rightarrow 0, \quad \varphi_1 \rightarrow 0 \end{aligned} \right\} \quad (25)$$

Solving Equations (19)-(24) subject to boundary conditions (25), we obtain:

$$F_0 = N_2 e^{-R_2 \eta} + N_3 e^{-R_1 \eta} + A_2 e^{-R_3 \eta}, \quad (26)$$

$$\left. \begin{aligned} F_1 &= N_{17} e^{-2R_2 \eta} + N_{18} e^{-2R_1 \eta} + N_{19} e^{-2R_3 \eta} + N_{20} e^{-(R_1+R_2)\eta} + N_{21} e^{-(R_1+R_3)\eta} \\ &\quad + N_{22} e^{-(R_2+R_3)\eta} + N_{23} e^{-R_1 \eta} + N_{24} e^{-R_2 \eta} + A_5 e^{-R_3 \eta} \end{aligned} \right\}, \quad (27)$$

$$\theta_0 = e^{-R_1 \eta}, \quad (28)$$

$$\theta_1 = N_4 e^{-2R_2 \eta} + N_5 e^{-2R_1 \eta} + N_6 e^{-2R_3 \eta} + N_7 e^{-(R_1+R_2)\eta} + N_8 e^{-(R_1+R_3)\eta} + N_9 e^{-(R_2+R_3)\eta} + A_3 e^{-R_1 \eta}, \quad (29)$$

$$\phi_0 = N_1 e^{-R_1 \eta} + A_1 e^{-R_2 \eta}, \quad (30)$$

$$\left. \begin{aligned} \phi_1 = & N_{10} e^{-2R_2 \eta} + N_{11} e^{-2R_1 \eta} + N_{12} e^{-2R_3 \eta} + N_{13} e^{-(R_1+R_2)\eta} + N_{14} e^{-(R_1+R_3)\eta} \\ & + N_{15} e^{-(R_2+R_3)\eta} + N_{16} e^{-R_1 \eta} + A_4 e^{-R_2 \eta} \end{aligned} \right\}. \quad (31)$$

By using Equations (26)–(31), we obtain the velocity, temperature, as well as concentration, as follows:

$$\left. \begin{aligned} F(\eta) = & N_2 e^{-R_2 \eta} + N_3 e^{-R_1 \eta} + A_2 e^{-R_3 \eta} + EcN_{17} e^{-2R_2 \eta} + EcN_{18} e^{-2R_1 \eta} + EcN_{19} e^{-2R_3 \eta} \\ & + EcN_{20} e^{-(R_1+R_2)\eta} + EcN_{21} e^{-(R_1+R_3)\eta} + EcN_{22} e^{-(R_2+R_3)\eta} + EcN_{23} e^{-R_1 \eta} \\ & + EcN_{24} e^{-R_2 \eta} + EcA_5 e^{-R_3 \eta} \end{aligned} \right\}, \quad (32)$$

$$\left. \begin{aligned} \theta(\eta) = & e^{-R_1 \eta} + EcN_4 e^{-2R_2 \eta} + EcN_5 e^{-2R_1 \eta} + N_6 e^{-2R_3 \eta} + EcN_7 e^{-(R_1+R_2)\eta} + EcA_3 e^{-R_1 \eta} \\ & + EcN_8 e^{-(R_1+R_3)\eta} + EcN_9 e^{-(R_2+R_3)\eta} \end{aligned} \right\}, \quad (33)$$

$$\left. \begin{aligned} \phi(\eta) = & N_1 e^{-R_1 \eta} + A_1 e^{-R_2 \eta} + EcN_{10} e^{-2R_2 \eta} + EcN_{11} e^{-2R_1 \eta} + EcN_{12} e^{-2R_3 \eta} + EcA_4 e^{-R_2 \eta} \\ & + EcN_{13} e^{-(R_1+R_2)\eta} + EcN_{14} e^{-(R_1+R_3)\eta} + EcN_{15} e^{-(R_2+R_3)\eta} + EcN_{16} e^{-R_1 \eta} \end{aligned} \right\}. \quad (34)$$

3.1 | Skin-friction

The skin-friction at the plate, which in the nondimensional form, is given by:

$$C_f = \left[1 + \frac{1}{\beta} \right] \left[\frac{\tau_w}{\rho U_0 V_0} \right] = \left[1 + \frac{1}{\beta} \right] \left[\frac{\partial u^*}{\partial y^*} \right]_{y=0}, \quad (35)$$

$$= - \left(\begin{aligned} & R_2 \eta N_2 + R_1 \eta N_3 + R_3 \eta A_2 + 2R_2 \eta EcN_{17} + 2R_1 \eta EcN_{18} + 2R_3 \eta EcN_{19} \\ & + (R_1 + R_2) \eta EcN_{20} + (R_1 + R_3) \eta EcN_{21} + (R_2 + R_3) \eta EcN_{22} + R_1 \eta EcN_{23} \\ & + R_2 \eta EcN_{24} + R_3 \eta EcA_5 \end{aligned} \right). \quad (36)$$

3.2 | Nusselt number

The rate of heat transfer coefficient, which in the nondimensional for, in terms of the Nusselt number is given by:

$$Nu = -x \left[\frac{\partial T^*}{\partial y^*} \right]_{y=0} \left[T_w^* - T_\infty^* \right]^{-1} \Rightarrow Nu Re_x^{-1} = - \left[\frac{\partial \theta}{\partial y} \right]_{y=0}, \quad (37)$$

$$\theta(\eta) = - \left(\begin{aligned} & R_1 \eta + 2R_2 \eta EcN_4 + 2R_1 \eta EcN_5 + 2R_3 \eta N_6 + (R_1 + R_2) \eta EcN_7 + R_1 \eta EcA_3 \\ & + (R_1 + R_3) \eta EcN_8 + (R_2 + R_3) \eta EcN_9 \end{aligned} \right). \quad (38)$$

3.3 | Sherwood number

The rate of mass transfer coefficient, which in the nondimensional form, in terms of the Sherwood number, is given by:

$$S_h = -x \left[\frac{\partial C^*}{\partial y^*} \right]_{y=0} \left[C_w^* - C_\infty^* \right]^{-1} \Rightarrow S_h \text{Re}_x^{-1} = - \left[\frac{\partial C}{\partial y} \right]_{y=0}, \quad (39)$$

$$\phi(\eta) = - \left(\begin{aligned} &R_1 \eta N_1 e^{-R_1 \eta} + R_2 \eta A_1 e^{-R_2 \eta} + 2R_2 \eta Ec N_{10} + R_1 \eta Ec N_{11} + R_3 \eta Ec N_{12} + R_2 \eta Ec A_4 \\ &+ (R_1 + R_2) \eta Ec N_{13} + (R_1 + R_3) \eta Ec N_{14} + (R_2 + R_3) \eta Ec N_{15} + R_1 \eta Ec N_{16} \end{aligned} \right). \quad (40)$$

4 | RESULTS AND DISCUSSION

To examine the influence of dissimilar flow estimators such as thermal Grashof (Gr), Soret (So), Prandtl number (Pr), heat generation parameter (Q), chemical reaction (Kr), Eckert number (Ec), mass Grashof (Gm), Schmidt number (Sc), Hall (β_i), ion-slip (β_e), Casson fluid (β), dimensionless viscosity (γ), porous (K), magnetic field (M), skin friction, and Nusselt and Sherwood parameters are determined analytically in two dimensionless viscosity cases ($\gamma = 1$ & -1) and exemplified with the aid of graphs. To solve the governing couple of nonlinear PDEs of the present problem, multiple regular perturbation method is required. For this reason, it was solved analytically and graphs were drawn by using Matlab 2008 version and where the x -axis is taken along the plate and the y -axis is normal to the plate. It is considered that x varies from 0 to 25 and y varies from 0 to 25. The dissimilar values of solute Grashof number (Gm) explained in two different cases (ie, $\gamma = -1$ & $\gamma = 1$) on the velocity are shown in Figure 2. From this figure, it reflects that disparate enhancement values of Gm lead to increase in velocity in case of dimensionless viscosity $\gamma = -1$ owing to the velocity distribution perpetrate an extreme value in the region and is then reduced to move in the direction of a free stream value. But a reverse effect occurred in case of dimensionless viscosity is unity (ie, $\gamma = 1$). This indicates that the motion of fluid precipitated owing to melioration in mass buoyancy force. Figure 3 illustrates that the enhancement of dissimilar values of (Gr) thermal Grashof number leads to rise in velocity due to intensification in buoyancy force in case of dimensionless viscosity $\gamma = -1$, but in case of $\gamma = 1$, the velocity diminished at the same values of Gr causes, the thermal Grashof number evinces the proportionate influence of the thermal buoyancy force in the boundary

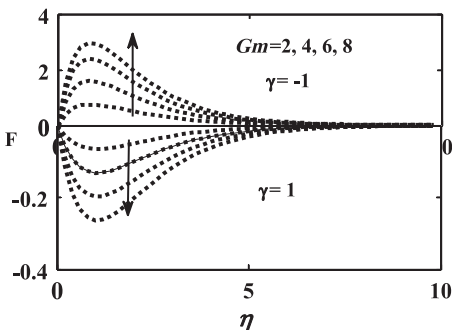


FIGURE 2 Plot of velocity $F(\eta)$ for varying Gm . $Pr = 7$; $Ec = 0.003$; $Sc = 0.60$; $M = 0.2$; $Kr = 0.2$; $K = 0.2$; $Gr = 2$; $So = 0.2$; $Q = 0.003$; $\beta = 2$; $\beta_e = 2$; $\beta_i = 2$

FIGURE 3 Plot of velocity $F(\eta)$ for varying Gr . $Pr = 7$; $Ec = 0.003$; $Sc = 0.60$; $M = 0.2$; $Kr = 0.2$; $K = 0.2$; $Gm = 2$; $So = 0.2$; $Q = 0.003$; $\beta_e = 2$; $\beta_i = 0.5$

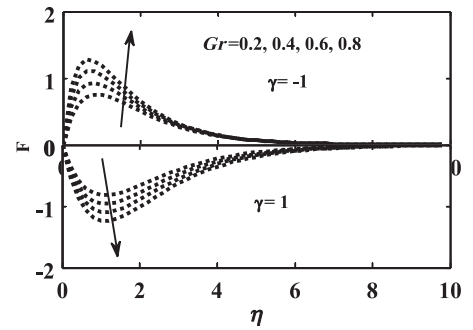
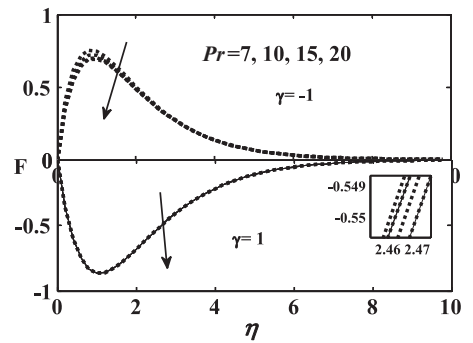


FIGURE 4 Plot of velocity $F(\eta)$ for varying Gr . $Ec = 0.003$; $Sc = 0.60$; $M = 0.2$; $Kr = 0.2$; $K = 0.2$; $Gm = 2$; $Gr = 2$ $So = 0.2$; $Q = 0.003$; $\beta_e = 2$; $\beta_i = 0.5$



layer. As a consequence of this amplification of thermal buoyancy force enforcement on the fluid particles for gravitational force, there is a rise in the thickness of momentum boundary layer. Figure 4 and Figure 15 show that for dissimilar values of Prandtl number ($Pr = 7, 10, 15, 20$; Kataria et al¹⁷) rises then it leads to reduced in velocity as well as temperature, When other parameters are rigid. In heat transfer problems, the Prandtl number restrains thickness of the momentum along with thermal boundary layers. This is owing to the reality that a higher Prandtl number fluid has comparatively low thermal conductivity, which diminishes the conduction as an outcome temperature reduces. Obviously, this is owing to the fluid by means of high Prandtl number has more and more viscosity, which diminishes thermal boundary layer thickness, that is, for declining thermal boundary layer, heat transfer is diminished. The dissimilarity of velocity, temperature as well as concentration for various values of the solet number So are shown in Figure 5, Figure 14 and Figure 23. In case of $\gamma = -1$, it is evidently

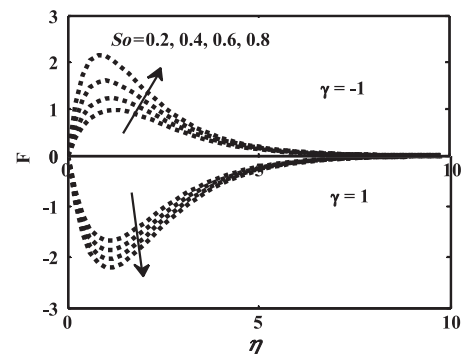


FIGURE 5 Plot of velocity $F(\eta)$ for varying So . $Pr = 7$; $Ec = 0.003$; $Sc = 0.60$; $M = 0.2$; $Kr = 0.2$; $K = 0.2$; $Gm = 2$; $Q = 0.003$; $\beta_e = 2$; $\beta_i = 0.5$

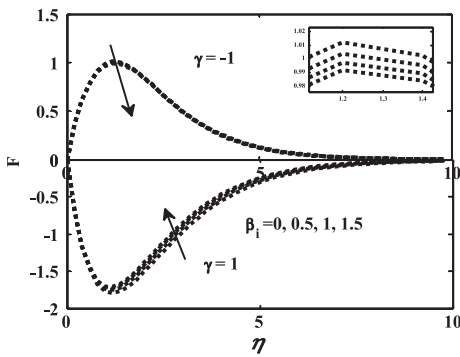


FIGURE 6 Plot of velocity $F(\eta)$ for varying β_i . $Pr = 7$; $Ec = 0.003$; $Sc = 0.60$; $M = 0.2$; $Kr = 0.2$; $K = 0.2$; $Gm = 2$; $Gr = 2$; $So = 0.2$; $Q = 0.003$; $\beta_e = 2$

seen that the velocity in the boundary layer rises by means of the enhancement of Soret number. From this figure, it was concluded that the fluid velocity rises owing to larger thermal diffusion. But inverse effect has been revealed in case of dimensionless viscosity $\gamma = 1$. Meanwhile, Figure 14 displays distinction of temperature for diverse values of Soret parameter So . In this figure, it was observed that the enhancement of dissimilar estimator's of Soret parameter leads to rise in temperature. The Soret number defines the influence of the temperature gradients, which show considerable mass diffusion effects. It is seen that the enhancement of Soret number leads to rise in the temperature within the boundary layer. Concurrently, representative dissimilarity of the concentration along the spanwise coordinate y are exhibited in Figure 23. From this figure, it was recognized that for diverse values of Soret parameter So rises; then it leads to a significant rise in concentration. The emphasis of Hall current and ion slip is indispensable in the presence of a strong magnetic field. Consequently, in numerous physical situations, it is obligatory to incorporate the influence of Hall current and ion slip terms in the MHD Casson fluid equations. Figure 6 shows the rise in velocity due to enhancement of diverse values of ion-slip parameter β_i in case of dimensionless viscosity $\gamma = 1$. But in case of $\gamma = -1$, the velocity diminished despite the incremental values of ion slip parameter β_i due to the fact that the β_i reduced the resistive force inflicted by the magnetic field. However from Figure 20, indistinguishable concrete outcomes appeared, wherein temperature. Figure 7 and Figure 19 represent the behavior of velocity as well as temperature for enhancement of dissimilar values of Hall parameter β_e . From this figure, it was found that the enhancement in various values of Hall parameter leads to reduced velocity and it is very near to the plate in case of dimensionless viscosity $\gamma = -1$ due to the production of an extra prospective dissimilarity transverse to the direction of accumulate free charge and applied magnetic field among the opposite surfaces

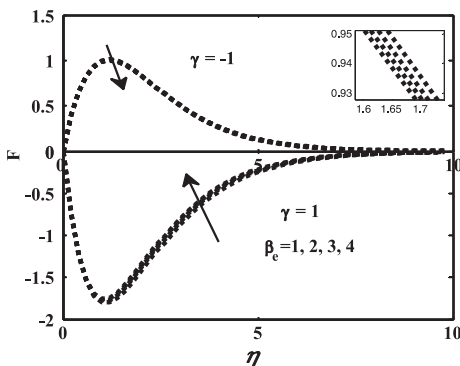
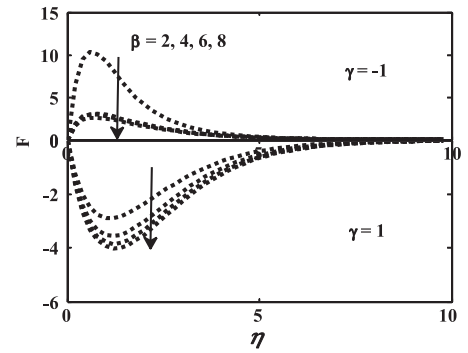


FIGURE 7 Plot of velocity $F(\eta)$ for varying β_e . $Pr = 7$; $Ec = 0.003$; $Sc = 0.60$; $M = 0.2$; $Kr = 0.2$; $K = 0.2$; $Gm = 2$; $Gr = 2$; $So = 0.2$; $Q = 0.003$; $\beta_i = 0.5$

FIGURE 8 Plot of velocity $F(\eta)$ for varying β . $Pr = 7$; $Ec = 0.003$; $Sc = 0.60$; $M = 0.2$; $Kr = 0.2$; $K = 0.2$; $Gm = 2$; $Gr = 2$; $So = 0.2$; $Q = 0.003$; $\beta_e = 2$; $\beta_i = 0.5$



induces an electric current vertical to both the fields, magnetic as well as electric. But an opposite effect occurred in case of dimensionless viscosity $\gamma = 1$. However, in Figure 19, it can be seen that the same outcomes occurred in case of temperature. Figure 8 depicts the distinction of velocity for diverse values of Casson fluid parameter in both cases. At this juncture, from the figure, it was seen that in both cases $\gamma = -1$ and $\gamma = 1$, the velocity is diminished due to the incremental values of β . Physically, by raising the Casson parameter that curtails the yield stress squelches the fluid velocity, that is, it generates resistance force in the fluid flow. It is observed that when the Casson parameter β is large enough, certain non-Newtonian attitudes evaporate and the fluid purely behaves like a Newtonian fluid. Thus, the velocity boundary layer thickness for Casson fluid is waistline than the Newtonian fluid. It takes place considering the plasticity of Casson fluid. The plasticity of the fluid magnifies with abatement in Casson parameter. Figures 9 and 16 confirm the influence of Eckert number (Ec) on the velocity and temperature. Figure 9 reveals that dissimilar augmentation values of Ec lead to a rise in velocity in both cases, that is, $\gamma = -1$ and $\gamma = 1$. Nevertheless, Figure 16 illustrates the influence of Eckert number on the temperature. From this figure it was identified that rise in the values of Ec leads to rise in temperature. Because the constructive Eckert number implies the cooling of the plate that is dissipation of heat from the plate to the fluid. The fact is that, higher viscous dissipative heat, for the reason that levitate in the fluid temperature and which is noticeable from Figure 16. The Eckert number characterizes the proportion between the flow of kinetic energy as well as enthalpy distinction of boundary layer. It signifies the restoration of kinetic energy into interior energy by means of work done against the viscous fluid stresses. The influence of disparate estimators of magnetic field M on the velocity illustrated in Figure 10. It can be distinguished that the velocity ascended by means of the rise in magnetic field parameter M in two cases

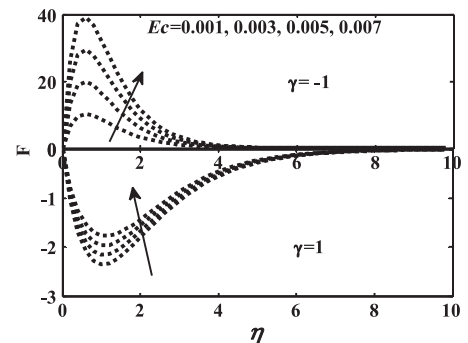


FIGURE 9 Plot of velocity $F(\eta)$ for varying Ec . $Pr = 7$; $Sc = 0.60$; $M = 0.2$; $Kr = 0.2$; $K = 0.2$; $Gr = 2$; $Gm = 2$; $So = 0.2$; $Q = 0.003$; $\beta = 2$; $\beta_e = 2$; $\beta_i = 2$

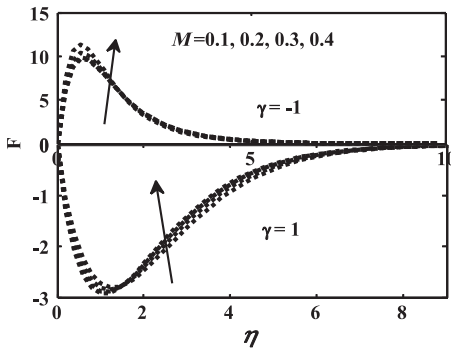


FIGURE 10 Plot of velocity $F(\eta)$ for varying M . $Pr = 7$; $Ec = 0.003$; $Sc = 0.60$; $Kr = 0.2$; $K = 0.2$; $Gr = 2$; $Gm = 2$; $So = 0.2$; $Q = 0.003$; $\beta = 2$; $\beta_e = 2$; $\beta_i = 2$

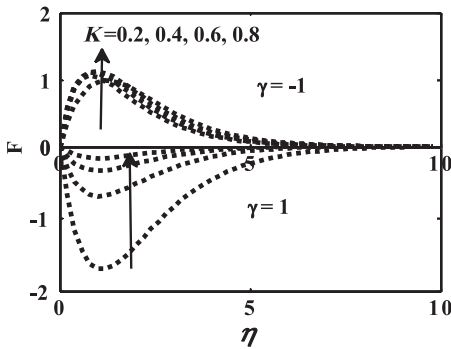


FIGURE 11 Plot of velocity $F(\eta)$ for varying K . $Pr = 7$; $Ec = 0.003$; $Sc = 0.60$; $M = 0.2$; $Kr = 0.2$; $Gr = 2$; $Gm = 2$; $So = 0.2$; $Q = 0.003$; $\beta = 2$; $\beta_e = 2$; $\beta_i = 2$

dimensionless viscosity $\gamma = -1$ and $\gamma = 1$ owing to the transverse retrenchment of momentum boundary layer is due to the applied magnetic field which consequences in the Lorentz force generating substantial resistance to the motion. Figure 11 shows the consequence of porous medium parameter K on the velocity. In this figure, based on the outcomes, it was found that the enhancement of K leads to rise in velocity in case of dimensionless viscosity $\gamma = 1$ as well as $\gamma = -1$. This is because of the existence of the porous medium in the flow furnishes confrontation to flow. Consequently, the resulting resistive force tends to slow down the motion of the fluid along the surface of the plate. Figures 12 and 22 exhibit the influence of chemical reaction parameter on velocity as well as concentration. Here the incremental values of Kr lead to rise in velocity in case of dimensionless viscosity $\gamma = 1$. This causes the chemical reaction to improve momentum transfer, while consequently accelerating the flow. But inverse effects were found in case of $\gamma = -1$, which means the enhancement of Kr leads to reduced velocity. And

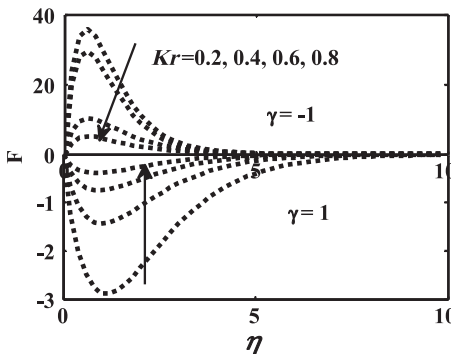


FIGURE 12 Plot of velocity $F(\eta)$ for varying Kr . $Pr = 7$; $Ec = 0.003$; $M = 0.2$; $K = 0.2$; $Gr = 2$; $Gm = 2$; $So = 0.2$; $Q = 0.003$; $\beta = 2$; $\beta_e = 2$; $\beta_i = 2$

FIGURE 13 Plot of velocity $F(\eta)$ for varying Sc . $Pr = 7$; $Ec = 0.003$; $M = 0.2$; $Kr = 0.2$; $K = 0.2$; $Gr = 2$; $Gm = 2$; $So = 0.2$; $Q = 0.003$; $\beta = 2$; $\beta_e = 2$; $\beta_i = 2$

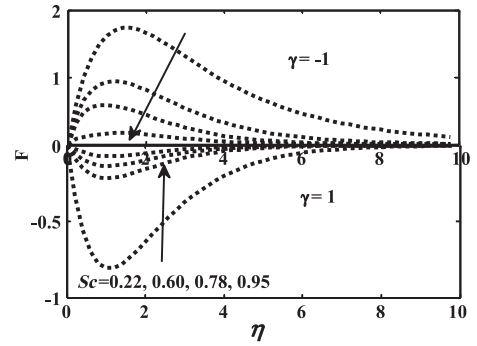


Figure 22 demonstrates the performance of concentration for disparate estimators of chemical reaction (Kr). The results obtained from this figure show that the concentration reduced due to rise in chemical reaction parameter. This is because the chemical reaction reinforces momentum transfer and consequently accelerates the flow. Figure 13 demonstrates the distinction of velocity for the influence of Schmidt number. The outcomes presented in figure indicate that for disparate values of Sc ascends then it causes decline in velocity in case of dimensionless viscosity $\gamma = -1$. Because the influence of concentration buoyancy to reduce yielding depletion in the fluid velocity. Depletions in the velocity distributions are accompanied by instantaneous reductions in the velocity boundary layers. But a reverse effect was observed in case of dimensionless viscosity $\gamma = 1$. The main causes for this effect are that the incremental values of Kr lead to rise in the many of solute molecules undergoing chemical reaction which reduced the solute field. Meanwhile for incongruent estimators of the Schmidt number on the fluid concentration is exposed in Figure 20. From this figure, the outcomes indicates that the enhancement of Sc leads to diminished in concentration. The values of Schmidt number considered vary the existence of species by hydrogen ($Sc = 0.22$), water vapor $Sc = 0.60$), ammonia ($Sc = 0.78$), and carbondioxide ($Sc = 0.95$). This causes the influence of concentration buoyancy to diminish, yielding a decline in the velocity. The depletion in the concentration is accompanied by instantaneous depletion in the concentration boundary layers, which is observable from Figure 21. The influence of heat generation parameter Q on the temperature is portrayed in Figure 17. In this figure, reduction in temperature due to reduction in heat generator parameter Q along the boundary layer was observed. This is because electrical energy is transformed resistively into heat. Physically, interruption, the existence of heat absorption effects has the propensity to reduce the temperature. Figure 18 depicts the influence of Casson

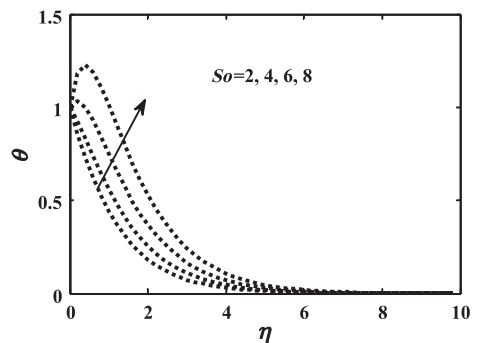


FIGURE 14 Plot of temperature $\theta(\eta)$ for varying So . $Pr = 7$; $Ec = 0.003$; $Sc = 0.60$; $M = 0.2$; $Kr = 0.2$; $K = 0.2$; $Gm = 2$; $Gr = 2$; $Q = 0.003$; $\beta = 2$; $\beta_e = 2$; $\beta_i = 2$

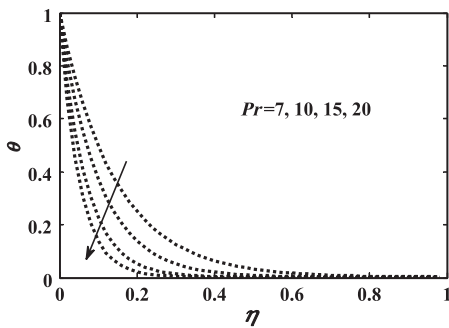


FIGURE 15 Plot of temperature $\theta(\eta)$ for varying Pr .
 $Ec = 0.003$; $Sc = 0.60$; $M = 0.2$; $Kr = 0.2$; $K = 0.2$; $Gr = 2$;
 $Gm = 2$; $So = 0.2$; $Q = 0.003$; $\beta = 2$; $\beta_e = 2$; $\beta_i = 2$

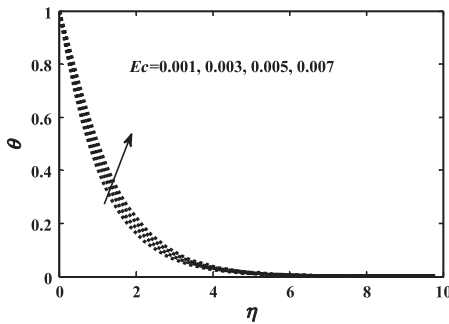


FIGURE 16 Plot of temperature $\theta(\eta)$ for varying Ec .
 $Pr = 7$; $Sc = 0.60$; $M = 0.2$; $Kr = 0.2$; $K = 0.2$; $Gr = 2$; $Gm = 2$;
 $So = 0.2$; $Q = 0.003$; $\beta = 2$; $\beta_e = 2$; $\beta_i = 2$

fluid model parameter on the temperature. The results obtain in this figure established that the temperature is declined due to disparate enhancement values of Casson fluid parameter β . Because diminished yield stress vanquishes the fluid temperature field. Figures 24-28 illustrate the comprehensive picture of skin friction. These figures indicate that the enhancement of Soret (So), Eckert number (Ec), and Grashof number for heat transform (Gm) leads to reduction in skin friction, but a reverse effect has been shown in case of Gr and β_e . Figures 29-32 demonstrate the influence of heat transfer coefficients on dissimilar parameters. From these figures, it was pore over N_w raises by enhancing the value of Eckert number Ec , Soret number So , and Prandtl number Pr . But a reverser effect was observed in case of Casson fluid parameter. Moreover, rate of heat transfer is higher in enormity in suction effects as contrasted to mass blowing or no mass transfer. Most imperative is, rate of heat transfer is greater underneath the effect of unsteady as compared to steady models. The influence of mass transfer coefficients,

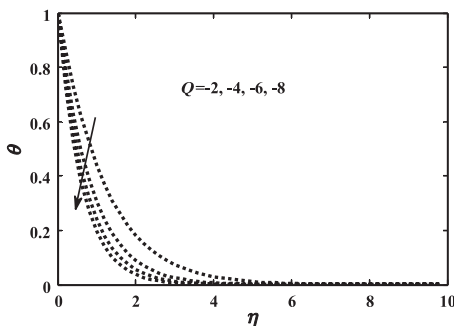


FIGURE 17 Plot of temperature $\theta(\eta)$ for varying Q .
 $Pr = 7$; $Ec = 0.003$; $Sc = 0.60$; $M = 0.2$; $Kr = 0.2$; $K = 0.2$;
 $Gr = 2$; $Gm = 2$; $So = 0.2$; $\beta = 2$; $\beta_e = 2$; $\beta_i = 2$

FIGURE 18 Plot of temperature $\theta(\eta)$ for varying β .
 $Pr = 7$; $Ec = 0.003$; $Sc = 0.60$; $M = 0.2$; $Kr = 0.2$; $K = 0.2$;
 $Gr = 2$; $Gm = 2$; $So = 0.2$; $Q = 0.003$; $\beta_e = 2$; $\beta_i = 2$

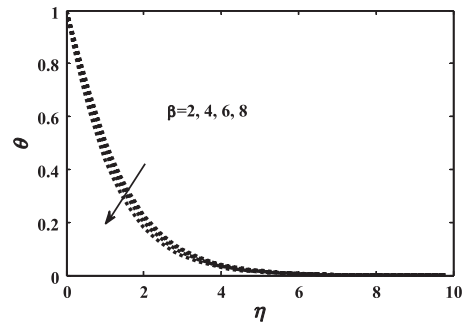


FIGURE 19 Plot of temperature $\theta(\eta)$ for varying β_e .
 $Pr = 7$; $Ec = 0.003$; $Sc = 0.60$; $M = 0.2$; $Kr = 0.2$; $K = 0.2$;
 $Gr = 2$; $Gm = 2$; $So = 0.2$; $Q = 0.003$; $\beta = 2$; $\beta_i = 2$

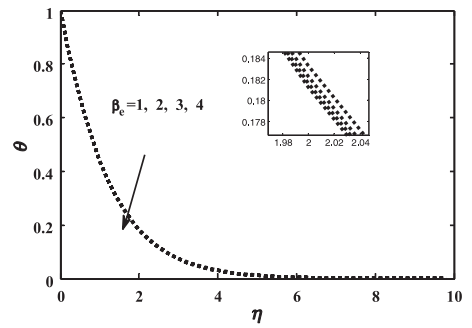


FIGURE 20 Plot of temperature $\theta(\eta)$ for varying β_i .
 $Pr = 7$; $Ec = 0.003$; $Sc = 0.60$; $M = 0.2$; $Kr = 0.2$; $K = 0.2$;
 $Gr = 2$; $Gm = 2$; $So = 0.2$; $Q = 0.003$; $\beta = 2$; $\beta_e = 2$

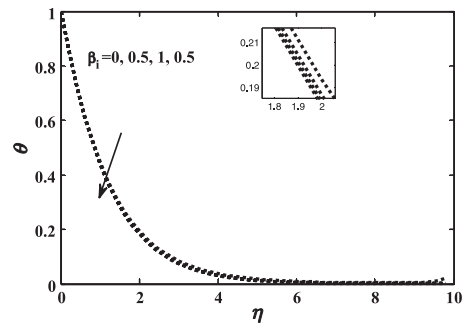
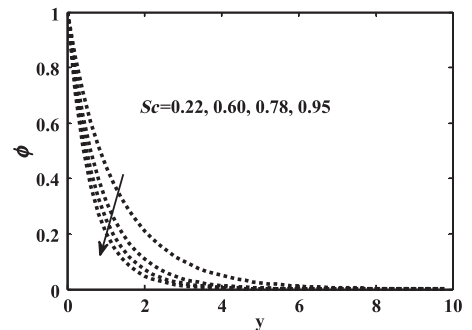


FIGURE 21 Plot of concentration $\phi(\eta)$ for varying Sc .
 $Pr = 7$; $Ec = 0.003$; $M = 0.2$; $Kr = 0.2$; $K = 0.2$; $Gr = 2$; $Gm = 2$;
 $So = 0.2$; $Q = 0.003$; $\beta = 2$; $\beta_e = 2$; $\beta_i = 2$



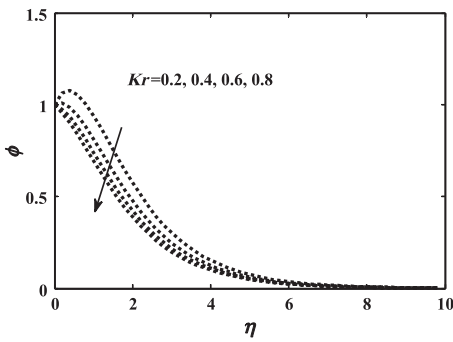


FIGURE 22 Plot of Concentration $\phi(\eta)$ for varying Kr .
 $Pr = 7$; $Ec = 0.003$; $Sc = 0.60$; $M = 0.2$; $K = 0.2$; $Gr = 2$;
 $Gm = 2$; $So = 0.2$; $Q = 0.003$; $\beta = 2$; $\beta_e = 2$; $\beta_i = 2$

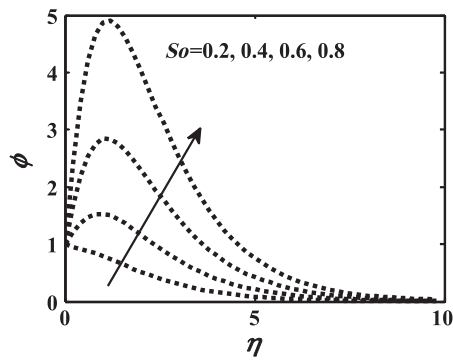


FIGURE 23 Plot of concentration $\phi(\eta)$ for varying So .
 $Pr = 7$; $Ec = 0.003$; $Sc = 0.60$; $M = 0.2$; $Kr = 0.2$; $K = 0.2$;
 $Gm = 2$; $Gr = 2$; $Q = 0.003$; $\beta = 2$; $\beta_e = 2$; $\beta_i = 2$

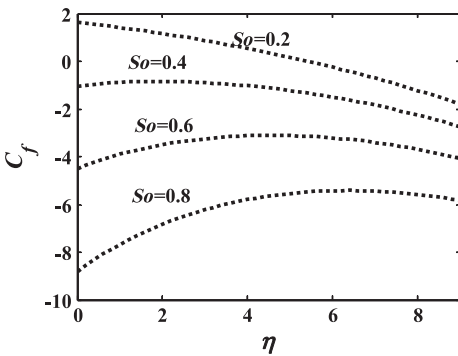


FIGURE 24 Plot of skin friction $C_f(\eta)$ for varying So .
 $Pr = 7$; $Ec = 0.003$; $Sc = 0.60$; $M = 0.2$; $Kr = 0.2$; $K = 0.2$;
 $Gm = 2$; $Gr = 2$; $Q = 0.003$; $\beta = 2$; $\beta_e = 2$; $\beta_i = 2$

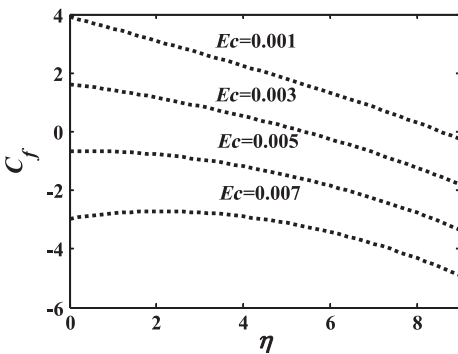


FIGURE 25 Plot of skin friction $C_f(\eta)$ for varying Ec .
 $Pr = 7$; $Sc = 0.60$; $M = 0.2$; $Kr = 0.2$; $K = 0.2$; $Gm = 2$; $Gr = 2$;
 $So = 0.2$; $Q = 0.003$; $\beta = 2$; $\beta_e = 2$; $\beta_i = 2$

FIGURE 26 Plot of skin friction $C_f(\eta)$ for varying Gm .
 $Pr = 7$; $Ec = 0.003$; $Sc = 0.60$; $M = 0.2$; $Kr = 0.2$; $K = 0.2$;
 $Gr = 2$; $So = 0.2$; $Q = 0.003$; $\beta = 2$; $\beta_e = 2$; $\beta_i = 2$

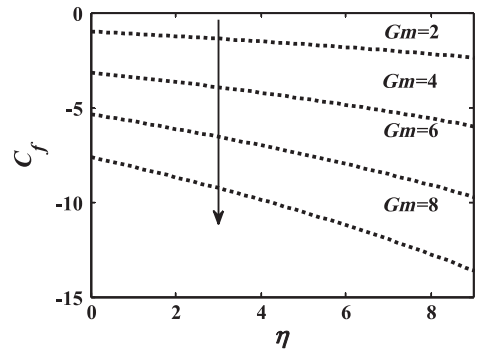


FIGURE 27 Plot of skin friction $C_f(\eta)$ for varying Gr .
 $Pr = 7$; $Ec = 0.003$; $Sc = 0.60$; $M = 0.2$; $Kr = 0.2$; $K = 0.2$;
 $Gm = 2$; $So = 0.2$; $Q = 0.003$; $\beta = 2$; $\beta_e = 2$; $\beta_i = 2$

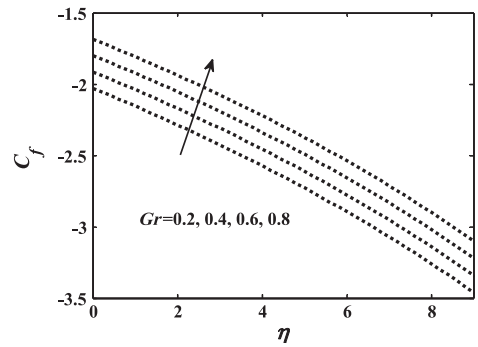


FIGURE 28 Plot of skin friction $C_f(\eta)$ for varying β_e .
 $Pr = 7$; $Ec = 0.003$; $Sc = 0.60$; $M = 0.2$; $Kr = 0.2$; $K = 0.2$;
 $Gm = 2$; $Gr = 2$; $So = 0.2$; $Q = 0.003$; $\beta = 2$; $\beta_i = 2$

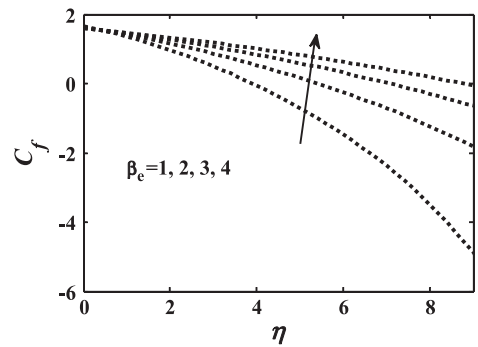
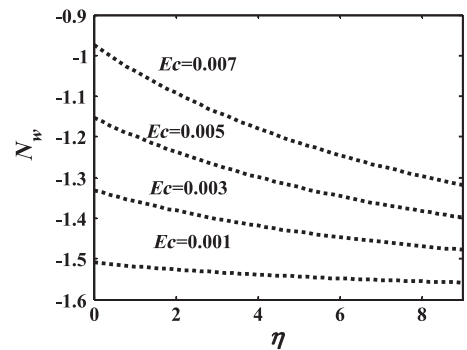


FIGURE 29 Plot of Nusselt number $N_w(\eta)$ for varying Ec . $Pr = 7$; $Sc = 0.60$; $M = 0.2$; $Kr = 0.2$; $K = 0.2$; $Gm = 2$;
 $Gr = 2$; $So = 0.2$; $Q = 0.003$; $\beta = 2$; $\beta_e = 2$; $\beta_i = 2$



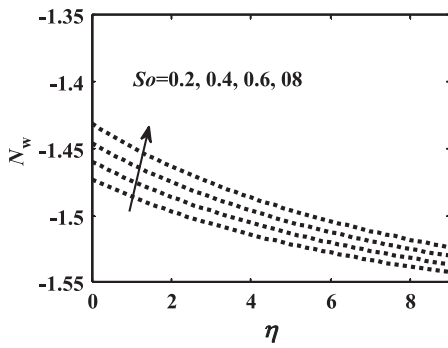


FIGURE 30 Plot of Nusselt number $N_w(\eta)$ for varying So . $Pr = 7$; $Ec = 0.003$; $Sc = 0.60$; $M = 0.2$; $Kr = 0.2$; $K = 0.2$; $Gm = 2$; $Gr = 2$; $Q = 0.003$; $\beta = 2$; $\beta_e = 2$; $\beta_i = 2$

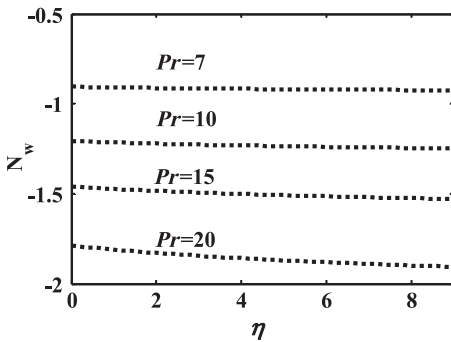


FIGURE 31 Plot of Nusselt number $N_w(\eta)$ for varying Pr . $Ec = 0.003$; $Sc = 0.60$; $M = 0.2$; $Kr = 0.2$; $K = 0.2$; $Gm = 2$; $Gr = 2$; $So = 0.2$; $Q = 0.003$; $\beta = 2$; $\beta_e = 2$; $\beta_i = 2$

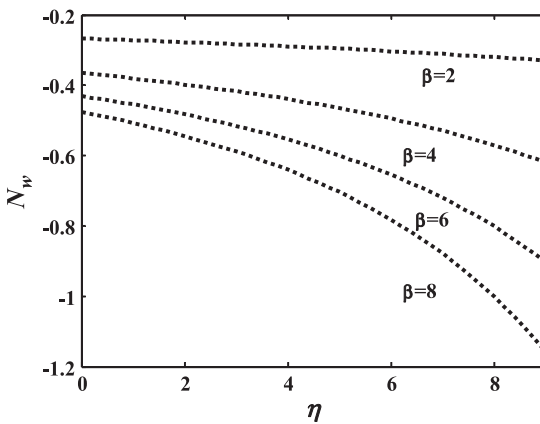


FIGURE 32 Plot of Nusselt number $N_w(\eta)$ for varying β . $Pr = 7$; $Ec = 0.003$; $Sc = 0.60$; $M = 0.2$; $Kr = 0.2$; $K = 0.2$; $Gm = 2$; $Gr = 2$; $So = 0.2$; $Q = 0.003$; $\beta_e = 2$; $\beta_i = 2$

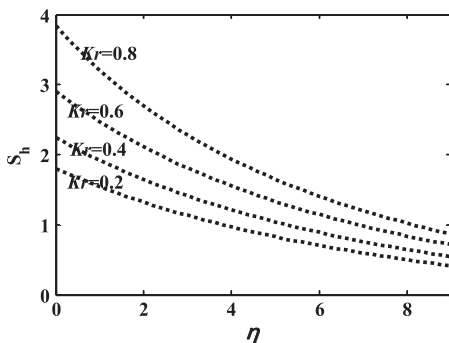


FIGURE 33 Plot of Sherwood $S_h(\eta)$ for varying Kr . $Pr = 7$; $Ec = 0.003$; $Sc = 0.60$; $M = 0.2$; $K = 0.2$; $Gm = 2$; $Gr = 2$; $So = 0.2$; $Q = 0.003$; $\beta = 2$; $\beta_e = 2$; $\beta_i = 2$

FIGURE 34 Plot of Sherwood $S_h(\eta)$ for varying Sc . $Pr = 7$; $Ec = 0.003$; $M = 0.2$; $Kr = 0.2$; $K = 0.2$; $Gm = 2$; $Gr = 2$; $So = 0.2$; $Q = 0.003$; $\beta = 2$; $\beta_e = 2$; $\beta_i = 2$

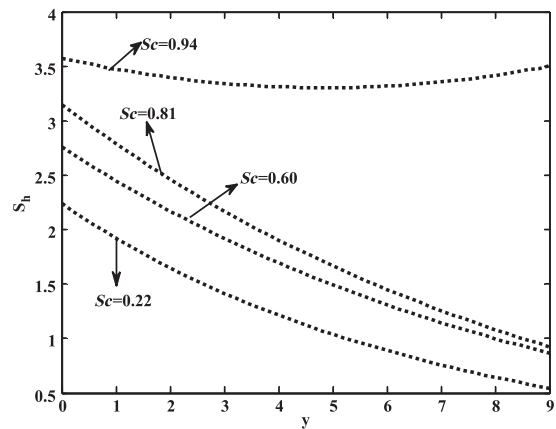


FIGURE 35 Plot of Sherwood $S_h(\eta)$ for varying So . $Pr = 7$; $Ec = 0.003$; $Sc = 0.60$; $M = 0.2$; $Kr = 0.2$; $K = 0.2$; $Gm = 2$; $Gr = 2$; $Q = 0.003$; $\beta = 2$; $\beta_e = 2$; $\beta_i = 2$

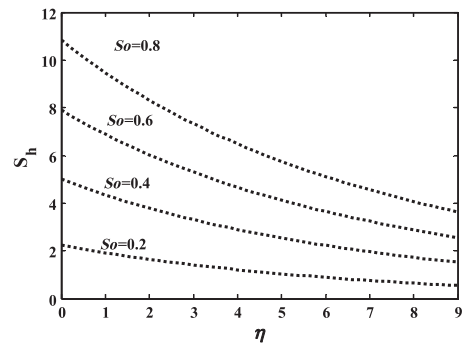


TABLE 1 Effect of various physical parameters on skin friction and Nusselt number

When nonappearance of Hall, ion-slip current				Mohammed Ibrahim et al ³²		Present study	
when	Gr	Gm	M	C_f	N_w	C_f	N_w
$Pr = 0.71$	3.0	1.0	1.0	2.5427	-0.5877	2.5427110	-0.5877321
$Ec = 0.001$	5.0	1.0	1.0	3.8114	-0.5854	3.8114341	-0.585415
$Q = 0.1$	7.0	1.0	1.0	5.0871	-0.5823	5.0871213	-0.582312
$Sc = 0.6$	1.0	1.0	1.0	3.8502	-0.5852	3.8502302	-0.585222
$Kr = 0.1$	3.0	3.0	1.0	5.1416	-0.5818	5.1416120	-0.581828
$So = 0.5$	5.0	5.0	1.0	1.2210	-0.5888	1.2210312	-0.588880
$\gamma = 0$	1.0	1.0	1.0	0.7695	-0.5892	0.7695214	-0.589222
as $\beta \rightarrow \infty$	3.0	1.0	3.0	2.3090	-0.5882	2.3090332	-0.588212
	5.0	1.0	5.0	2.1306	-0.5885	2.1306213	-0.588542

that is, Sherwood number $S_h(\eta)$ on diverse values on Figures 33-35. From these figures, it was understandable that Sherwood number is decline by enhancing the dissimilar estimators of chemical reaction Kr , Schmidt number Sc , and Soret number So .

5 | VALIDATION OF THE RESULTS

In this study, it should be mentioned that the outcomes obtained herein are compared with the results of Mohammed Ibrahim et al.³² in the nonappearance of Hall, ion-slip current, Casson fluid on skin friction and Nusselt number taking dissimilar values for Grashof number (Gr), solutal Grashof number (Gm), and magnetic field M , keeping the other parameters fixed and these results are presented in Table 1. The comparison exhibits a good agreement.

6 | CONCLUSIONS

- Dissimilar increment in Gm , Gr , and So lead to rise in velocity in case of $\gamma = -1$. But a reverse effect was observed in case of $\gamma = 1$.
- Increase in various values of the chemical reaction parameter Kr leads to decline in velocity in case of $\gamma = -1$. But a reverse effect was observed in case of $\gamma = 1$.
- Velocity rises due to enhancement of diverse values of ion-slip parameter β_i in case of $\gamma = 1$. But velocity is reduced in case of $\gamma = -1$ even with the incremental values of ion slip parameter β_i . However a reverser effect has been shown in case of Hall parameter β_e .
- Velocity profile is diminished due to the incremental values of Casson fluid parameter β as well as Prandtl number Pr in both cases $\gamma = -1$ and $\gamma = 1$.
- The fluid velocity rises with the dissimilar incremental values of Eckert number Ec , porous parameter K and magnetic field M in velocity in both cases, that is $\gamma = -1$ & $\gamma = 1$.
- The fluid velocity reduced with incremental values of Schmidt number Sc in case of $\gamma = -1$. However a reverse effect was seen in case of $\gamma = 1$.
- The fluid temperature reduces with the increasing values of heat source parameter. But a reverse effect was seen in case of Eckert number Ec .
- The concentration diminishes by means of the enhancement values of Schmidt number Sc and Chemical reaction Kr . But an inverse effect was observed in case of Soret number (So).
- The Sherwood number $S_h(\eta)$ declines with enhancing dissimilar estimators of chemical reaction Kr , Schmidt number (Sc), and Soret number (So).
- The skin friction is diminished with the increasing values of Soret (So), Eckert number (Ec), and Grashof number for heat transform (Gm) but a reverse effect has been shown in case of Gr and β_e .
- The enhancement of Soret (So), Eckert (Ec), and Grashof number for heat transform (Gm) leads to reduced in skin friction, but reverse effect has been shown in case of Gr and β_e .

ACKNOWLEDGMENT

The authors are thankful to the referee for his valuable suggestions, which helped to improve the quality of this manuscript.

NOMENCLATURE

B_0	magnetic induction (A/m)
C	nondimensional concentration

C_p	specific heat for constant pressure($\text{J}\cdot\text{kg}^{-1}\cdot\text{K}$)
C_w^*	concentration of the plate (kg/m^3)
C_f	local skin-friction (N/m)
C_∞^*	concentration in the fluid far away from the plate (kg/m^3)
D	chemical molecular diffusivity (m^2/s)
D_1	coefficient of thermal diffusivity
e	electron charge (C)
E	electric field intensity (V/m)
Ec	Eckert number
g^*	acceleration due to gravity (m/s^2)
Gm	solulal Grashof number
Gr	local temperature Grashof number
J	current density (A/m^2)
K	permeability of porous medium
Kr	chemical reaction parameter (m/s)
k_e^*	mean absorption coefficient
k	thermal conductivity ($\text{W}\cdot\text{m}^{-1}\cdot\text{K}^{-1}$)
K_1	chemical reaction rate constant
M	magnetic parameter
N_u	Nusselt number
p_y	yield stress of fluid
Pr	Prandtl number
Q_0	heat generation/absorption
q_r^*	radiation heat flux density (W/m^2)
Ra	thermal radiation parameter
R^*	radiation parameter
S_h	Sherwood number
Sc	Schmidt number
So	Soret
T_∞	dimensional free stream temperature (K)
T^*	dimensional temperature (K)
t^*	dimensional time (S)
T	temperature of the fluid (K)
T_w	fluid temperature at walls (K)
T_∞	dimensional free stream temperature (K)
T_w^*	fluid temperature at the wall (K)
u_p^*	direction of fluid flow
U_0	reference velocity at the plate (m/s)
U_∞^*	free stream velocity (K)
u	components of velocity vector in x direction (m/s)
v	velocity component in y-direction (m/s)
v^*	scale of suction velocity
V_0	scale of suction velocity (m/s)
x^*, y^*	coordinate axis along the plate (m), coordinate axis normal to the plate (m)

GREEK SYMBOLS

β_e	Hall current parameter
α^*	shear rate
F	complex velocity
ω_e	cyclotron frequency(Hz)
β	Casson fluid parameter
β^*	coefficient of volumetric expansion (m^3/kg)
γ	dimensionless viscosity
μ	fluid dynamic viscosity
ρ	density of the fluid (kg/m^3)
ϑ	fluid kinematic viscosity (m^2/s)
ε	scalar constant ($\ll 1$)
β_i	ion-slip parameter
σ	electrical conductivity ($\Omega^{-1} \cdot \text{m}^{-1}$)
σ_s^*	Stefan-Boltzmann constant ($\text{W} \cdot \text{m}^{-2} \cdot \text{K}^{-4}$)
τ_w	skin-friction coefficient (m^2/s)
τ_0	Casson yield stress
μ_B	plastic dynamic viscosity
τ_e	electron collision time (s)
ν_r	kinematic rotational viscosity

SUBSCRIPTS

P	plate
∞	free stream condition
W	wall condition
*	dimensionless properties

ORCID

K. V. B. Rajakumar  <http://orcid.org/0000-0002-2667-8042>

M. Umasankara Reddy  <http://orcid.org/0000-0003-2828-8053>

REFERENCES

1. Biswas R, Mondal M, Islam A. A steady MHD natural convection heat transfer fluid flow through a vertical surface in the existence of Hall current and radiation. *Instrumentation Mesure Métrologie*. 2019;17(2):331-356.
2. Biswas R, Afikuzzaman M, Mondal M, Ahmmed SF. MHD free convection and heat transfer flow through a vertical porous plate in the presence of chemical reaction. *Front Heat Mass Transfer*. 2018; 11(13):1-10.
3. Ahmmed SF, Biswas R. Effects of radiation and chemical reaction on MHD unsteady heat and mass transfer of nanofluid flow through a vertical plate. *Model Measure Control B*. 2019;87(4):213-220.
4. John Etwire C, Yakubu Seini I, Abe-I-Kpeng G. MHD flow of Casson fluid over a vertical plate embedded in porous media with joule heating and convective boundary condition. *Asian J Math Comput Res*. 2017;19(2): 50-64.
5. Mittal AS, Patel HR. Influence of thermophoresis and Brownian motion on mixed convection two dimensional MHD Casson fluid flow with non-linear radiation and heat generation. *Stat Mech Appl*. 2020;537(1):1-15.
6. Patel HR. Effects of cross diffusion and heat generation on mixed convective MHD flow of Casson fluid through porous medium with non-linear thermal radiation. Vol. 5, Pp:1-26, no. 4, 2019.
7. Kataria HR, Patel HR. Heat and mass transfer in magnetohydrodynamic Casson fluid flow past over an oscillating vertical plate embedded in porous medium with ramped wall temperature. *Propul Power Res*. 2018;7(3):257-267.

8. Vinod Kumar G, Kiran Kumar R, Varma SVK. Multiple slips and chemical reaction effects on MHD stagnation point flow of Casson fluid over a stretching sheet with viscous and joules heating. *Frontiers Heat Mass Transfer*. 2018;10(23):105-115.
9. Prasad KV, Vajravelu K, Hanumesh V, Rashidi M, Neelufar. Flow and heat transfer of a Casson liquid over a vertical stretching surface: optimal solution. *Am J Heat Mass Transfer*. 2018;5(1):1-22.
10. Ullah I, Khan I, Shafie S. Heat and mass transfer in unsteady MHD slip flow of Casson fluid over a moving wedge embedded in a porous medium in the presence of chemical reaction. *Numer Methods Partial Differ Equations*. 2017;35(5):1867-1891.
11. El-Aziz MA, Afify AA. Influences of slip velocity and induced magnetic field on MHD stagnation-point flow and heat transfer of Casson fluid over a stretching sheet. *Hindawi Math Prob Eng*. 2018;1:1-11.
12. Biswas R, Mondal M, Sarkar DR, Ahmmed SF. Effects of radiation and chemical reaction on MHD unsteady heat and mass transfer of Casson fluid flow past a vertical plate. *J Adv Math Comput Sci*. 2017;23(2):1-16.
13. Biswas R, Hasan M, Mondal M, Kazi Shanchia M, Bulbul F, Ahmmed SF. A numerical superintendence with stability exploration of Casson nanofluid flow in the effects of variable thermal conductivity and radiation. *Adv Sci Engi Med*. 2019;11(8):697-707.
14. Biswas R, Mondal M, Shanchia K, Ahmed R, Abdus Samad SK, Ahmmed SF. Explicit finite difference analysis of an unsteady magnetohydrodynamics heat and mass transfer micropolar fluid flow in the presence of radiation and chemical reaction through a vertical porous plate. *J Nanofluids*. 2019;8(2):1583-1591.
15. Srinivas S, Kumar CK, Reddy AS. Pulsating flow of Casson fluid in a porous channel with thermal radiation, chemical reaction and applied magnetic field. *Nonlinear Anal Model Control*. 2018;23(2):213-233.
16. Sobamowo MG. Combined effects of thermal radiation and nano particles on free convection flow and heat transfer of Casson fluid over a vertical plate. *Int J Chem Eng*. 2018;18:1-25.
17. Kataria HR, Patel HR. Effects of chemical reaction and heat generation/absorption on MHD Casson fluid flow over an exponentially accelerated vertical plate embedded in porous medium with ramped wall temperature and ramped surface concentration. *Propul Power Res*. 2019;8(1):35-46.
18. Ahmmed SF, Biswas R, Afikuzzaman M. Unsteady MHD free convection flow of nano fluid through an exponentially accelerated inclined plate embedded in a porous medium with variable thermal conductivity in the presence of radiation. *J Nanofluids*. 2018;7(5):891-901.
19. Vijaya N, Hari Krishna Y, Kalyani K. Soret and radiation effects on unsteady flow of a Casson fluid through porous vertical channel with expansion and contraction. *Front Heat Mass Transfer*. 2018;11(19):1-20.
20. Biswas R, Ahmmed SF. Effects of Hall current and chemical reaction on MHD unsteady heat and mass transfer of Casson nanofluid flow through a vertical plate. *J Heat Transfer*. 2018;140(9):1-12.
21. Mondal M, Biswas M, Hasan M, Kazi S, Ahmmed SF. Numerical investigation with stability convergence analysis of chemically hydromagnetic casson nanofluid flow in the effects of thermophoresis and Brownian motion. *Int J Heat Technol*. 2019;37(1):59-70.
22. Reddy GJ, Srinivasa Raju R, Rao JA. Influence of viscous dissipation on unsteady MHD natural convective flow of Casson fluid over an oscillating vertical plate. *Ain Shams Eng J*. 2017;5(1):1-9.
23. Attia HA. Transient MHD Couette flow of a Casson fluid between parallel plates with heat transfer. *Italian J Pure Appl Math*. 2010;27(1):19-38.
24. Srinivasa Raju R, Reddy J. Anita MHD Casson viscous dissipative fluid flow past a vertically inclined plate in presence of heat and mass transfer. *Front Heat Mass transfer*. 2017;8(27):1-12.
25. Saidulu N, Lakshman AV. MHD Flow of Casson fluid with slip effects over an exponentially porous stretching sheet in presence of thermal radiation, viscous dissipation and heat source/sink. *Am Res J Math*. 2016;2(1):1-15.
26. Srinivasa RR, Reddy BM, Reddy GJ. Influence of angle of inclination on unsteady MHD Casson fluid flow past a vertical surface filled by porous medium in presence of constant heat flux, chemical reaction and viscous dissipation. *J Nanofluids*. 2017;6(4):668-679.
27. El-Aziz MA, Afify AA. Influences of slip velocity and induced magnetic field on MHD stagnation-point flow and heat transfer of Casson fluid over a stretching sheet. *Hindawi Math Prob Eng*. 2018;18:1-11.
28. Abo-Eldahab EM, El Aziz MA. Viscous dissipation and Joule heating effects on MHD-free convection from a vertical plate with power-law variation in surface temperature in the presence of Hall and ios-slips currents. *Appl Math Model*. 2005;29(2):579-595.

29. Barletta A, Celliv M. Mixed convection MHD flow in a vertical channel. *Int J Heat Mass Transfer*. 2008;5(4): 6110-6117.
30. Babu VS, Reddy GVR. Mass transfer effects on MHD mixed convective flow from a vertical surface with ohmic heating and viscous dissipation. *Adv Appl Sci Res*. 2011;2(4):138-146.
31. Chien-Hsin C. Combined heat and mass transfer in MHD free convection from a vertical surface with ohmic heating and viscous dissipation. *Int J Eng Sci*. 2004;42(7):699-13.
32. Mohammed Ibrahim S, Suneetha K. Heat source and chemical effects on MHD convection flow embedded in a porous medium with Soret, viscous, and Joules dissipation. *Ain Shams Eng J*. 2016;7(2):811-818.
33. Patel HR, Singh R. Thermophoresis, Brownian motion and non-linear thermal radiation effects on mixed convection MHD micropolar fluid flow due to nonlinear stretched sheet in porous medium with viscous dissipation, joule heating and convective boundary conditions. *Int Commun Heat Mass Transfer*. 2019;107:68-92.
34. Mittal AS, Patel HR, Darji RR. Mixed convection micropolar ferrofluid flow with viscous dissipation, joule heating and convective boundary conditions. *Int Commun Heat Mass Transfer*. 2019;108:1-15.
35. Biswas R, Mondal M, Hossain S, Kazi FU, Suma UK, Katun M. A numerical investigation with hydro-magnetic stability convergence analysis on unsteady heat and mass transfer fluid flow through a vertical porous plate. *Adv Sci Eng Med*. 2019;11:687-696.
36. Balamurugan KS, Varma SVK, Krishna Prasad KR, Iyengar SN. Dissipation, chemical reaction and thermo-diffusion effects on MHD free convection flow through porous medium with constant suction. *Int J Adv Sci Technol*. 2011;3(4):113-131.
37. Pannerselvi R, Kowsalya J. Ion slip and dufour effect on unsteady free convection flow past an infinite vertical plate with oscillatory suction velocity and variable permeability. *Int J Sci Res*. 2015;4(12):2079-2090.
38. Abuga JG, Kinyanjui M, Sigey JK. An investigation of the effect of hall currents and rotational parameter on dissipative fluid flow past a vertical semi-infinite plate. *J Eng Technol Res*. 2011;3(1):314-320.
39. Ojjela O, Nedunuri NK. Hall and ion slip effects on free convection heat and mass transfer of chemically reacting couple stress fluid in a porous expanding or contracting walls with Soret and Dufour effects. *Front Heat Mass Transfer*. 2014;5(22):1-12.
40. Motsa SS, Sibanda P. The effects of thermal radiation, hall currents, Soret, and Dufour on MHD flow by mixed convection over a vertical surface in porous media. *Math Prob Eng*. 2010;2010:1-20.
41. Patel HR. Effects of heat generation, thermal radiation and hall current on MHD Casson fluid flow past an oscillating plate in porous medium. *Multiphase Sci Technol*. 2019;3(1):87-107.
42. Vijayaragavan R, Karthikeyan S. Hall current effect on chemically reacting MHD Casson fluid flow with dufour effect and thermal radiation. *Asian J Appl Sci Technol*. 2018;2(2):228-245.
43. Anika N, Hoque M, Hossain I. Thermal diffusion effect on unsteady viscous MHD micropolar fluid flow through an infinite vertical plate with hall and ion-slip current. *Procedia Eng*. 2015;105(1):160-166.
44. Srinivasacharya D, Shafeeurrahaman Md. Mixed convection flow of nanofluid in a vertical channel with hall and ion-slip effects. *Front Heat Mass Transfer*. 2017;8(11):1-8. <https://doi.org/10.5098/hmt.8.11>
45. Rajakumar KVB, Balamurugan KS, Ramana Murthy ChV. The radiation, dissipation and Dufour effects on MHD free convection Casson fluid flow through a vertical Oscillatory porous plate with Ion-slip current. *Int J Heat Technol*. 2018;36(2):494-508.
46. Rajakumar KVB, Balamurugan KS, Ramana Murthy ChV. Viscous dissipation and dufour effects on MHD free convection flow through an oscillatory inclined porous plate with hall and ion-slip current. *Int J Eng Technol*. 2018;7(4.5):410-415.
47. Rajakumar K V B, Balamurugan KS, Ramana Murthy ChV Radiation, dissipation and Dufour effects on MHD free convection flow through a vertical oscillatory porous plate with ion-slip current. Numerical Heat Transfer and Fluid Flow, Lecture Notes in Mechanical engineering, Springer Nature Singapore Pte Ltd. Select Proceedings of NHTFF 2018 (pp. 587-596) 2019.

How to cite this article: Rajakumar KVB, Umasankara Reddy M, Balamurugan KS, Raja Ram KVBS. Steady MHD Casson Ohmic heating and viscous dissipative fluid flow past an infinite vertical porous plate in the presence of Soret, Hall, and ion-slip current. *Heat Transfer*. 2020;1–30. <https://doi.org/10.1002/hjt.21680>

APPENDIX

$$\begin{aligned}
R_1 &= \frac{\text{Pr} + \sqrt{(\text{Pr})^2 - 4\text{Pr}Q}}{2}, \quad R_2 = \frac{Sc + \sqrt{(Sc)^2 - 4ScKr}}{2}, \quad R_3 = \frac{1 + \sqrt{1 + 4\left[1 + \frac{1}{\beta} + \gamma\right]N}}{2} \\
N_1 &= \frac{-R_1^2 ScSo}{R_1^2 - ScR_1 - ScKr}, \quad N_2 = \frac{-GmA_1}{\left[1 + \frac{1}{\beta} + \gamma\right]R_2^2 - R_2 - N}, \quad N_3 = \frac{-Gr - GmN_1}{\left[1 + \frac{1}{\beta} + \gamma\right]R_1^2 - R_1 - N}, \\
N_4 &= \frac{-\text{Pr}\left[1 + \frac{1}{\beta}\right]N_2^2 R_2^2 - \text{Pr}\left[\frac{M^2}{[\alpha_e^2 + \beta_e^2]}\right]\left[1 + \frac{1}{\beta}\right]N_2^2}{4R_2^2 - 2\text{Pr}R_2 + \text{Pr}Q} \quad N_5 = \frac{-\text{Pr}\left[1 + \frac{1}{\beta}\right]R_1^2 N_3^2 - \left[1 + \frac{1}{\beta}\right]\left[\frac{M^2}{[\alpha_e^2 + \beta_e^2]}\right]\text{Pr}N_3^2}{4R_1^2 - 2\text{Pr}R_1 + \text{Pr}Q} \\
N_6 &= \frac{-\text{Pr}\left[1 + \frac{1}{\beta}\right]A_2^2 R_3^2 - \text{Pr}\left[1 + \frac{1}{\beta}\right]\left[\frac{M^2}{[\alpha_e^2 + \beta_e^2]}\right]A_2^2}{4R_3^2 - 2\text{Pr}R_3 + \text{Pr}Q}, \\
N_7 &= \frac{-2R_1 R_2 N_2 N_3 \left[1 + \frac{1}{\beta}\right]\text{Pr} - 2\text{Pr}\left[1 + \frac{1}{\beta}\right]\left[\frac{M^2}{[\alpha_e^2 + \beta_e^2]}\right]N_3 N_2}{(R_1 + R_2)^2 - (R_1 + R_2)\text{Pr} + \text{Pr}Q} \\
N_8 &= \frac{-2R_1 R_3 A_2 N_3 \left[1 + \frac{1}{\beta}\right]\text{Pr} - 2\text{Pr}\left[1 + \frac{1}{\beta}\right]\left[\frac{M^2}{[\alpha_e^2 + \beta_e^2]}\right]A_2 N_3}{(R_1 + R_3)^2 - (R_1 + R_3)\text{Pr} + \text{Pr}Q} \\
N_9 &= \frac{-2A_2 R_3 R_2 N_2 \left[1 + \frac{1}{\beta}\right]\text{Pr} - 2\text{Pr}N_2 A_2 \left[1 + \frac{1}{\beta}\right]\left[\frac{M^2}{[\alpha_e^2 + \beta_e^2]}\right]}{(R_2 + R_3)^2 - (R_2 + R_3)\text{Pr}Q\text{Pr}} \\
N_{10} &= \frac{-4R_2^2 N_2 ScSo}{4R_2^2 - 2ScR_2 - ScKr}, \quad N_{11} = \frac{-4R_1^2 N_5 ScSo}{4R_1^2 - 2ScR_1 - ScKr}, \quad N_{12} = \frac{-4R_3^2 N_6 ScSo}{4R_3^2 - 2ScR_3 - ScKr} \\
N_{13} &= \frac{-(R_1 + R_1)^2 N_7 Sc So}{(R_1 + R_1)^2 - Sc(R_1 + R_1) - ScKr}, \quad N_{14} = \frac{-(R_1 + R_3)^2 N_8 Sc So}{(R_1 + R_3)^2 - Sc(R_1 + R_3) - ScKr} \\
N_{15} &= \frac{-(R_2 + R_3)^2 N_9 ScSo}{(R_2 + R_3)^2 - Sc(R_2 + R_3) - ScKr}, \quad N_{16} = \frac{-A_3 R_1^2 ScSo}{R_1^2 - ScR_1 - ScKr}, \\
N_{17} &= \frac{-GrN_4 - GmN_{10}}{4\left[1 + \frac{1}{\beta} + \gamma\right]R_2^2 - 2R_2 - N}
\end{aligned}$$

$$N_{18} = \frac{-GrN_5 - GmN_{11}}{4\left[1 + \frac{1}{\beta} + \gamma\right]R_1^2 - 2R_1 - N}, \quad N_{19} = \frac{-GrN_6 - GmN_{12}}{4\left[1 + \frac{1}{\beta} + \gamma\right]R_3^2 - 2R_3 - N}$$

$$N_{20} = \frac{-GrN_7 - GmN_{13}}{\left[1 + \frac{1}{\beta} + \gamma\right](R_1 + R_2)^2 - (R_1 + R_2) - N},$$

$$N_{21} = \frac{-GrN_8 - GmN_{14}}{\left[1 + \frac{1}{\beta} + \gamma\right](R_1 + R_3)^2 - (R_1 + R_3) - N}$$

$$N_{22} = \frac{-GrN_9 - GmN_{15}}{\left[1 + \frac{1}{\beta} + \gamma\right](R_3 + R_2)^2 - (R_3 + R_2) - N},$$

$$N_{22} = \frac{-GrN_9 - GmN_{15}}{\left[1 + \frac{1}{\beta} + \gamma\right](R_3 + R_2)^2 - (R_3 + R_2) - N}$$

$$N_{23} = \frac{-GrA_3 - GmN_{16}}{\left[1 + \frac{1}{\beta} + \gamma\right]R_1^2 - R_1 - N}, \quad N_{24} = \frac{-GmA_4}{\left[1 + \frac{1}{\beta} + \gamma\right]R_2^2 - R_2 - N}, \quad A_1 = (1 - N_1),$$

$$A_2 = (N_2 + N_3)$$

$$A_3 = -(N_4 + N_5 + N_6 + N_7 + N_8 + N_9), \quad A_4 = -(N_{10} + N_{11} + N_{12} + N_{13} + N_{14} + N_{15} + N_{16}),$$

$$A_5 = -(N_{17} + N_{18} + N_{19} + N_{20} + N_{21} + N_{22} + N_{23} + N_{24})$$